

ORGANIZATION FOR NUCLEAR RESEARCH

CERN-EP/86-119
September 8th, 1986

# COMPARISON BETWEEN HADRONIC FINAL STATES PRODUCED IN μp AND $e^+e^-$ INTERACTIONS

The European Muon Collaboration

Aachen[1], CERN[2], DESY (Hamburg)[3], Freiburg[4], Hamburg (University)[5], Kiel[6], LAL (Orsay)[7], Lancaster[8], LAPP (Annecy)[9], Liverpool[10], Marseille[11], Mons[12], MPI (München)[13], Oxford[14], RAL (Chilton)[15], Sheffield[16], Torino[17], Uppsala[18], Warsaw[19], Wuppertal[20].

M. Arneodo[17], A. Arvidson[18], J.J. Aubert[11], B. Badelek[19a)], J. Beaufays[2], C.P. Bee[8b)], C. Benchouk[11], G. Berghoff[1], I. Bird[8c)], D. Blum[7], E. Böhm[6], X. de Bouard[9], F.W. Brasse[3], H. Braun[20], C. Broll[9+)], S. Brown[10d)], H. Brück[20e)], H. Calen[18], J.S. Chima[15f)], J. Ciborowski[19a], R. Clifft[15], G. Coignet[9], F. Combley[16], J. Coughlan[8g)], G. D'Agostini[11], S. Dahlgren[18], F. Dengler[13], I. Derado[13], T. Dreyer[4], J. Drees[20], M. Düren[1], V. Eckardt[13], A. Edwards[20h)], M. Edwards[15], T. Ernst[4], G. Eszes[9i)], J. Favier[9], M.I. Ferrero[17], J. Figiel[5j)], W. Flauger[3], J. Foster[16k)], E. Gabathuler[10], J. Gajewski[5], R. Gamet[10], J. Gayler[3], N. Geddes[14l)], P. Grafström[18], F. Grard[12], J. Haas[4], E. Hagberg[18], F.J. Hasert[1m)], P. Hayman[10], P. Heusse[7], M. Jaffré[7], A. Jacholkowska[2], F. Janata[5], G. Jancso[13], A.S. Johnson[14n)], E.M. Kabuss[4], G. Kellner[2], V. Korbel[3], J. Krüger[20e)], S. Kullander[18], U. Landgraf[4], D. Lanske[1], J. Loken[14], K. Long[14o)], M. Maire[9], P. Malecki[13], A. Manz[13], S. Maselli[13], W. Mohr[4], F. Montanet[11], H.E. Montgomery[2p)], E. Nagy[9i)], J. Nassalski[19q)], P.R. Norton[15], F.G. Oakham[15r)], A.M. Osborne[2], C. Pascaud[7], B. Pawlik[13], P. Payre[11], C. Peroni[17], H. Peschel[20], H. Pessard[9], J. Pettingale[10], B. Pietrzyk[11], B. Pönsgen[5], M. Pötsch[20], P. Renton[14], P. Ribarics[9i)], K. Rith[4c)], E. Rondio[19a)], A. Sandacz[19q)], M. Scheer[1], A. Schlagböhmer[4], H. Schiemann[5], N. Schmitz[13], M. Schneegans[9], M. Scholz[1], T. Schröder[4], M. Schouten[13], K. Schultze[1], T. Sloan[8], H.E. Stier[4], M. Studt[5], G.N. Taylor[14], J.M. Thénard[9], J.C. Thompson[15], A. de la Torre[5s)], J. Toth[9i)], L. Urban[1], L. Urban[9i)], W. Wallucks[4], M. Whalley[16t)], S. Wheeler[16], W.S.C. Williams[14], S.J. Wimpenny[10o)], R. Windmolders[12], G. Wolf[13].

(Submitted to Zeits. für Physik C)

## Abstract

A comparison is made between the properties of the final state hadrons produced in 280 GeV μp interactions and in $e^+e^-$ annihilation. The Lund model of hadroproduction is used as an aid in understanding the differences observed. The hadron distributions from μp and $e^+e^-$ interactions are consistent with the quark parton model assumption of environmental independence, provided that the differences in heavy quark production and hard QCD effects in the two processes are taken into account. A comparison with a $K^+p$ experiment is also made. Values are also determined for the Lund model parameters $\sigma_q = 0.410 \pm 0.002 \pm 0.020$ GeV and $\sigma' = 0.29^{+.05\ +0.14}_{-.07\ -0.18}$ GeV, controlling the transverse momenta in fragmentation and intrinsic transverse momenta of the struck quark respectively.

For footnotes see next page

Addresses

1) III. Physikalisches Institut A, Physikzentrum, Aachen, Germany.
2) CERN, Geneva, Switzerland.
3) DESY, Hamburg, Germany.
4) Fakultät für Physik, Universität Freiburg, Germany.
5) II. Institut für Experimentalphysik, Universität Hamburg, Germany.
6) II. Institut für Kernphysik, Universität Kiel, Germany.
7) Laboratoire de l'Accélérateur Linéaire, Université de Paris-Sud, Orsay, France.
8) Department of Physics, University of Lancaster, England.
9) LAPP IN2P3, Annecy-le-Vieux, France.
10) Department of Physics, University of Liverpool, England.
11) Centre de Physique des Particules, Faculté des Sciences de Luminy, Marseille, France.
12) Faculté des Sciences, Université de L'Etat à Mons, Belgium.
13) Max-Planck-Institut für Physik und Astrophysik, München, Germany.
14) Nuclear Physics Laboratory, University of Oxford, England.
15) Rutherford and Appleton Laboratory, Chilton, Didcot, England.
16) Department of Physics, University of Sheffield, England.
17) Istituto di Fisica, Università di Torino, Italy.
18) Gustav Werners Institut, University of Uppsala, Sweden.
19) Physics Institute, University of Warsaw, and Institute for Nuclear Studies, Warsaw, Poland.
20) Fachbereich Physik, Universität Wuppertal, Germany.

a) University of Warsaw, Poland.
b) Now at University of Liverpool, England.
c) Now at MPI für Kernphysik, Heidelberg, Germany.
d) Now at TESA S.A., Renens, Switzerland.
e) Now at DESY, Hamburg, Germany.
f) Now at 30 Addison Ave., Hounslow, England.
g) Now at RAL, Chilton, Didcot, England.
h) Now at Jet, Joint Undertaking, Abingdon, England.
i) Now at Central Research Institute for Physics of the Hungarian Academy of Science, Budapest, Hungary.
j) Now at Institute of Nuclear Physics, Krakow, Poland.
k) Now at University of Manchester, England.
l) Now at British Telecom, London, England.
m) Now at Krupp Atlas Elektronic GmbH, Bremen, Germany.
n) Now at SLAC, Stanford, California.
o) Now at CERN, Geneva, Switzerland.
p) Now at FNAL, Batavia, Illinois, U.S.A.
q) Institute for Nuclear Studies, Warsaw, Poland.
r) Now at NRC, Ottawa, Canada.
s) Now at Universidad Nacional, Mar del Plata, Argentina.
t) Now at University of Durham, England.
+) Deceased.

## 1. Introduction

It is widely believed that the fundamental interactions of nature are describable by local gauge theories. Strong interactions can be described in terms of a local SU(3) colour gauge theory, Quantum Chromodynamics (QCD). Electroweak phenomena are described by the standard Glashow-Salam-Weinberg model. Of these theories, QCD is the least well understood and tested. The main difficulty in testing QCD is that the field quanta, the quarks, antiquarks and gluons, are not directly observed experimentally, so their properties must be inferred indirectly from those of the final state hadrons.

Two of the reactions in which the study of quarks and gluons is cleanest are $e^+e^-$ annihilation to hadrons and deep inelastic lepton-nucleon scattering. In the former, the simplest parton final state is a quark-antiquark pair, whereas in the latter an energetic quark or antiquark is knocked out of the nucleon leaving a spectator diquark or more complex target remnant system. The understanding of the underlying parton dynamics is difficult, however, because it appears that effects at the quark level are considerably diluted at the hadron level. This dilution stems from a variety of sources:

a) A given quark or gluon fragments into several hadrons. For example, a quark with an energy in the hadronic centre of mass system (cms) of 10 GeV has a mean hadronic multiplicity of about six.
b) There are considerable event to event fluctuations, both in the number of hadrons produced and in their momentum distribution with respect to the underlying parton axes in both the transverse and longitudinal directions.
c) A large fraction of the observed hadrons arise from the decays of short lived primary hadrons.
d) Although clear jet structures with limited transverse momenta ($< p_T > \sim$ 0.35 GeV) with respect to the jet axis are observed, it is difficult to assign particles which are slow in the cms to a particular jet with any degree of confidence. In order to minimise this uncertainty a cms energy (W) greater than 10 GeV is desirable for the study of 2-jet final states.
e) Many experiments have good detection efficiences only for charged hadrons.

Nonetheless the underlying quark properties are reflected in those of the hadrons into which they fragment. For example, in ref.[1] it was shown that the charge of the leading hadron in the fragmentation process is strongly correlated to the charge of the fragmenting quark. It is therefore of importance to ascertain to what extent the properties of the final state hadrons differ in these different reactions and to try to understand both the differences and the similarities in terms of QCD and the Quark Parton Model (QPM).

In this paper the properties of final state hadrons in 280 GeV $\mu^+p$ interactions are compared to those from other reactions, in particular $e^+e^-$ annihilation. The requirement that $W \geq 10$ GeV, which is in order to achieve reasonable separation of the jet fragments, limits the amount of available data to which the $\mu^+p$ results can be compared. The upper limit in the comparison, which arises from kinematic and acceptance considerations for the $\mu p$ data, is that $W \lesssim 20$ GeV.

The data from $e^+e^-$ annihilation are selected to correspond to the single photon intermediate state (fig. 1a). In the energy region $10 < W < 20$ GeV the contribution from the $Z^\circ$ boson is negligible. The energetic quark-antiquark pair is produced from a time-like virtual photon. The quarks are produced with a cross section which depends on the square of the quark charge, hence $u, d, s, c$, and $b$ quarks are produced in approximately the ratio 4:1:1:4:1. Thus about 73% of the final states arise from quarks and antiquarks of charge $\pm 2/3$. Fig. 1a represents the leading-order QCD process. The $O(\alpha_s)$ diagrams are shown in figs. 1b and c.

The deep inelastic $\mu^+p$ scattering process takes place predominantly via the one photon exchange diagram shown in fig. 2a. The scattering takes place on either a quark or an antiquark and the relative probability is again proportional to the square of the quark charge. Since the quark composition of a proton is $uud$, the scattering from the constituent valence quarks is mainly from $u$-quarks. The flavour of the struck quark depends on the value of the Bjorken scaling variable $x_{BJ}$. In terms of the four-momenta shown in fig. 2a, $x_{BJ} = Q^2/(2p.q)$, where $Q^2 = -q^2$. In the QPM, $x_{BJ}$ is the fraction of the protons four-momentum carried by the struck quark. At high values of $x_{BJ}$ the scattering is mainly off valence quarks (mostly $u$), whereas at low $x_{BJ}$ ( $\lesssim 0.1$) there is a large contribution from sea-quarks (mostly from $u$ and $\bar{u}$). The scattering process in the QPM involves the absorption of the virtual photon, which is space-like, by a quark or antiquark, after which the struck quark has a large momentum with respect to the remaining partons in the proton. The remnant partons are assumed to act as spectators in the collision. In the case of scattering off one of the valence quarks in the proton the remnant system is a diquark. The term diquark does not imply that the remnant quarks are bound together, although such a possibility is not excluded.

Deep inelastic scattering and $e^+e^-$ annihilation may be described in terms of QCD as follows. The energetic $q$ and $\bar{q}$ formed in $e^+e^-$ annihilation have a large momentum with respect to one another. A strong colour field between the quark (colour triplet) and the antiquark (colour antitriplet) will be formed. In $\mu^+p$ scattering a colour field will be formed between the struck quark (3 or $\bar{3}$ in colour) and the remaining system which is also 'coloured'. What happens next can, at present, only be approximated by models. It is assumed that the confining forces will result in the production of hadrons from the colour field and that this fragmentation process will take place over a distance of the order of fermis. Measurements of forward hadron production in $\mu p$ scattering on heavy nuclear targets [2] have shown that this fragmentation distance could be in excess of 10 fermis. Similarities in the properties of hadrons formed from such a colour field in $e^+e^-$ and $\mu p$ interactions are expected.

There are, however, differences between the two reactions which make a direct comparison more difficult to interpret. A significant fraction (~40%) of the $e^+e^-$ final states with $W \gtrsim 10$ GeV consist of a heavy $(c, b)$ $q\bar{q}$ pair, whereas heavy quark production is rather small (< 1%) in $\mu p$ interactions. Conservation of baryon number in $\mu p$ scattering requires that there is at least one final state baryon. This baryon is preferentially produced from the target remnant system [3] as expected in the QPM. For this reason the $e^+e^-/\mu p$ comparison is more

meaningful if restricted to those hadrons in $\mu p$ collisions which are produced in the quark fragmentation region. This region is chosen (somewhat arbitrarily) to be the forward hemisphere in the cms.

In $\mu p$ collisions the virtual photon direction, which is well measured experimentally, gives a natural axis with which to analyse final state hadrons. No such axis exists for the hadrons produced in $e^+e^-$ interactions and the event axis must be inferred from the hadrons themselves. The methods commonly used are to determine the sphericity (S) [4] or thrust (T) [5] axes. These methods do not, however, identify which of the jets arises from the quark rather than the antiquark, hence hadron distributions are usually folded into one hemisphere.

Another difference to be expected in an $e^+e^-/\mu p$ comparison is from hard QCD. The $O(\alpha_s)$ diagrams in $e^+e^-$ and $\mu^+p$ interactions involving an external gluon are shown in figs. 1b and 1c and in figs. 2b and 2c respectively. In addition to the diagrams shown there are also $O(\alpha_s)$ contributions to the total cross-section from diagrams containing gluon loops. For $e^+e^-$, both the quark and antiquark can radiate a gluon whereas radiation only occurs from the scattered quark for $\mu p$ interactions. The diagrams with gluon emission are also expected to influence the final state hadron production in the limit of soft multiple gluon radiation. Some evidence supporting these ideas in $\mu p$ scattering has been given in ref.[6]. At low values of $x_{BJ}$ there is a contribution to $\mu p$ from the photon-gluon fusion diagrams (figs. 2d and 2e) which has no analogue in $e^+e^-$ annihilation. A further difference is that in $\mu p$ scattering the struck quark or antiquark has a certain intrinsic or primordial transverse momentum, $k_T$. This can be considered to arise from the forces confining the quark inside the proton and is thus presumably related to higher order QCD processes.

In addition to a direct comparison of the $e^+e^-$ and $\mu p$ data the Lund string model [7] is used to try to understand the underlying physical processes. This model contains the QPM and QCD ideas outlined above and gives a reasonable description of the main features of both sets of data. It is useful in that particular features (heavy quark production, hard QCD effects, vector meson decays etc) can be switched off in the generation of the Monte Carlo events. Hence an estimate of the expected magnitude of a particular effect can be made. There are, however, a considerable number of parameters in the Lund model and, in section 3, the values used to simulate the $\mu p$ events are discussed. In section 4 an estimate is made of the parameters $\sigma'$ and $\sigma_q$ used to specify the widths of the intrinsic transverse momentum ($k_T$) and fragmentation transverse momentum distributions respectively. Section 2 contains the event and track selection procedures for $\mu p$ events and a discussion of possible systematic effects. The comparison with $e^+e^-$ annihilation is described in section 5, which also contains a discussion of the possible interpretation of the observed differences. In section 6 a comparison with some results from the scattering of $K$-mesons off protons is made. The conclusions are summarised in section 7.

## 2. Event selection and correction procedure

A detailed description of the detector and subsequent analysis procedures can be found in ref.[8]. A 280 GeV beam of positive muons is incident on a 1m long liquid hydrogen target, which is surrounded by a streamer chamber,

which in turn is positioned inside a superconducting vertex spectrometer magnet (VSM). The scattered muon and hadrons with momentum greater than about 5 GeV pass through a second magnet, the forward spectrometer magnet (FSM). The bending power of the FSM is roughly equal and opposite to that of the VSM. The two magnets are instrumented with proportional and drift chambers. The apparatus is triggered by fast scintillator hodoscopes when a muon is scattered through more than $^1/_2°$.

The data reduction, streamer chamber film measurement and off-line analysis (see ref.[8]) result in three classes of tracks, namely

i) Forward Spectrometer (FS) tracks. This class consists of the scattered muon and those fast ($p \gtrsim 5$ GeV) hadron tracks which traverse the FS magnet.

ii) Streamer Chamber (SC) tracks. These tracks are measured in the streamer chamber. In general SC tracks cover the low momentum part of the spectrum.

iii) Vertex System (VS) tracks. VS tracks are those found only in the detectors between the vertex and the forward spectrometer. These tracks (and also the FS tracks) are in the very forward direction and are generally not measurable in the streamer chamber as they are obscured by out of time beam tracks.

For tracks in categories i) and ii) the VS detectors are used, where possible, to improve the precision of track measurement. The fractions of FS, SC and VS tracks in the sample used are about 15%, 74% and 11%, respectively. Together, the track types cover a wide range of momentum from 280 GeV down to 200 MeV.

As the primary vertex is not visible in the streamer chamber it is determined by fitting the incident and scattered muons and any compatible charged hadron tracks. A search is also made amongst the charged hadron tracks (FS and SC) for any vertices consistent with arising from strange particle decays or $\gamma$ conversion, or from the secondary interaction of a hadron in the target or other material in the apparatus. In the present analysis, except where specifically indicated to the contrary, only hadrons from the primary vertex are taken into account. Thus hadrons arising from $K^\circ_s$, $\Lambda$ and $\bar{\Lambda}$ decays are not included.

The experiment contains an extensive particle identification system, consisting of a set of gas Cerenkov counters filled with neopentane and nitrogen for low and intermediate momenta hadron identification, aerogel Cerenkov counters and a time of flight hodoscope system for low momenta and a neon filled Cerenkov counter for fast forward particles. This system allows identification of roughly 50% of all charged hadrons. Further details and results on the $x_F$ distributions of identified charged particles can be found in refs. [3,8]. The particle identification is not used directly in this analysis.

Events are selected for further analysis if the following selection criteria

are satisfied:

$$Q^2 > 4 \text{ GeV}^2$$
$$W^2 > 20 \text{ GeV}^2$$
$$x_{BJ} > 0.01,\ y_{BJ} < 0.90$$
$$20 < \nu < 260 \text{ GeV}$$
$$E'_\mu > 20 \text{ GeV}$$
$$\theta_\mu > 0.75°$$

where $\nu = E_\mu - E'_\mu$, $y_{BJ} = \nu/E_\mu$. $E_\mu$ is the lab energy of the incident muon and $E'_\mu$ is the lab energy of the scattered muon, which subtends an angle $\theta_\mu$ with respect to the beam. The quantity $W$ is the centre of mass energy of the virtual photon-proton system and hence that of the outgoing hadrons. The quantities are based on the one photon exchange diagram shown in fig. 2a. The values of the cuts are chosen so as to eliminate kinematic regions where the correction factors for acceptance or radiative effects are large or rapidly varying.

The properties of the final state hadrons can be conveniently described in terms of the longitudinal ($p_L$) and transverse ($p_T$) components of the particle's momentum in the hadronic cms with respect to the virtual photon axis or some other estimator of the jet axis, e.g. sphericity. The following cms longitudinal variables are used

$$x_F = \frac{2p_L}{W}$$
$$y^* = \frac{1}{2}\ln\left(\frac{E + p_L}{E - p_L}\right).$$

All the distributions presented below have been corrected for the effects of acceptance, smearing introduced by the resolution of the apparatus, radiative effects and the efficiency of the various off-line pattern recognition, track fitting and vertex finding algorithms. These corrections are determined using a detailed Monte Carlo simulation of the experiment in which events were generated using the Lund string model [7] and imposing the kinematic selection criteria given above. A simulation of the raw data was made including the effects of film measurement and chamber inefficiencies, and the production of tracks by $\gamma$ conversions in all the material of the apparatus and secondary interactions of hadrons in the target. These simulated events were passed through the same analysis chain as the real events. For a particular distribution the correction function is then computed as the ratio of the original generated Monte Carlo distribution and that obtained after the experimental simulation. The errors arising from the finite statistics in the Monte Carlo are added to the statistical errors on the data.

The results presented below are given for charged particles in terms of the hadronic cms variables. The transformation from the laboratory system to the cms system requires knowledge of the particle's mass. The mass assignment for this transformation is as follows. All negative particles are assigned the pion mass. Positive particles with $x_F(\pi) > -0.2$ ($x_F(\pi)$ is the value of $x_F$ computed using the pion mass) are also assigned the pion mass. Positive particles with $x_F(\pi) < -0.2$ are assigned the proton mass unless $x_F(p) < -0.9$ in which case the pion mass is used. Based on studies using identified particles [3] and also

Monte Carlo simulated events, it is estimated that, throughout the whole $x_F$ range, $\gtrsim 75\%$ of the hadrons are correctly classified in this way. The same procedure is used in the Monte Carlo simulation of the experiment. Thus the correction function takes into account not only the effects of acceptance losses and smearing, but also the influence of residual wrong-mass assignments.

The Monte Carlo simulation does not fully account for all aspects of the data. Hence there exist some potential systematic effects. The inadequacies in the Monte Carlo are the lack of background hits in the tracking chambers, in particular in the 'noisy' region near the beam, and residual distortions in the streamer chamber optical parameterisation. Detailed studies have been carried out in order to estimate the possible systematic errors in the distributions presented below. These are described in ref.[9]. In the distributions presented below the statistical errors are shown by solid lines and the estimated total errors (statistical and systematic errors added in quadrature) are displayed, where shown, as extensions to the statistical errors.

## 3. Discussion of the values of the parameters in the Lund model

To facilitate the comparison of the data in $\mu p$ and $e^+e^-$ interactions it is useful also to compare the data to a model which contains the theoretical ingredients outlined in section 1. In this way the model can also be used as an aid in the interpretation of the data. The model which has been used for these purposes is the Lund string model [7]. This model contains several parameters which are not predicted directly by the model and which must be determined from the data. The values of the parameters used to generate events are discussed in this section.

In the case of $\mu p$ scattering the ratio of the production of primary vector and pseudoscalar mesons was set to $V/PS = 1$; this value is compatible with a measurement of the $\rho^\circ/\pi^\circ$ ratio in this reaction [10], namely $V/PS = 0.90 \pm 0.35(\text{stat.}) \,^{+0.35}_{-0.30}(\text{syst.})$. The relative production of $s\bar{s}$ to $u\bar{u}$ (or $d\bar{d}$) pairs was set to $\gamma_s/\gamma_u = 0.3$; this value gives a reasonable description of the production spectra of $K^\circ$ [11] and $K^\pm$ [3] mesons. The production spectra of $p$, $\bar{p}$, $\Lambda$ and $\bar{\Lambda}$ are adequately described using a value of $P_{qq}/P_q = 0.075$ for the parameter dictating the relative production of diquark-antidiquark to quark-antiquark pairs, together with the specific mechanism used to describe the target jet fragmentation to baryons[3]. The model also allows the inclusion of $O(\alpha_s)$ QCD corrections to the matrix elements. The transverse momentum distributions in and out of the event plane in a selected sample of 3-jet events are reasonably well described using a value for $\alpha_s \sim 0.3$ [12]. The soft gluon limit of the $O(\alpha_s)$ matrix element is also included. A study of the distribution in rapidity of the transverse momentum balancing that of the leading hadrons is well reproduced by this simulation of soft gluon effects [3,13]. Estimates of the values of the parameters $\sigma_q$, which parameterises the transverse momentum of quarks and antiquarks produced in the fragmentation of the string, and of $\sigma'$, the average intrinsic transverse momentum of the struck quark inside the proton, are discussed below.

In the case of the $e^+e^-$ annihilation there has been some effort in determining the values of the parameters in the Lund model. The JADE collabora-

tion [14] finds the values $V/PS = 1.04 \pm 0.18$ and $\gamma_s/\gamma_u = 0.27 \pm 0.06$. The TPC collaboration [15] finds $V/PS = 0.89 \pm 0.50$ and $\gamma_s/\gamma_u = 0.32 \pm 0.10$. The TASSO collaboration [16] use second order QCD corrections together with $\sigma_q = 0.453 \pm 0.014$ GeV, $V/PS = 1.38 \pm 0.96$ and $\gamma_s/\gamma_u = 0.35 \pm 0.05$ to fit various aspect of their data. For baryon production the model of Meyer [17] is used with a value of $P_{qq}/P_q = 0.11$.

Despite the uncertainties in the values of the parameters discussed above the Lund model gives, for a fixed set of parameters, a reasonable description of a wide class of data. Differences in the values of the parameters in different experiments or different reactions can stem from either possible correlations amongst the parameters or the sensitivity of an experiment to particular ingredients of the model, as well as possible inadequacies of the model. It should be stressed that attempts to understand the fragmentation process, when the properties of the underlying partons can only be indirectly inferred from the hadron properties, are necessarily difficult. Although the Lund model may not correspond to physical reality, many of its postulates are supported by the data. Thus the model provides a framework for the comparison of different reactions and it is in this context that it will be used below.

## 4. Determination of $\sigma_q$ and $\sigma'$

The transverse momentum distribution of the quarks and antiquarks produced by the fragmentation of the colour field of the string is given in the Lund model by

$$\frac{d\sigma}{dp_\perp^2} \propto e^{-p_\perp^2/\sigma_q^2}$$

where $p_\perp$ is measured with respect to the string axis. The intrinsic transverse momentum $k_T$ of the struck quark leads essentially to a rotation of the event axis of the final state system with the current and target fragments having contributions in opposite directions for a particular event. The form used to parameterise the distribution of $k_T$ is*

$$\frac{d\sigma}{dk_T^2} \propto e^{-k_T^2/\sigma'^2} \quad .$$

In order to estimate the parameters $\sigma_q$ and $\sigma'$ it is desirable to find measurable quantities which are sensitive to these parameters whilst being relatively insensitive to the other parameters of the model. The quantity used in this analysis which is sensitive to $\sigma_q$ is

$$\delta q = \left| \left(\underline{p}_T\right)_1 - \left(\underline{p}_T\right)_2 \right|$$

where $\left(\underline{p}_T\right)_1$ and $\left(\underline{p}_T\right)_2$ are the transverse momenta of two hadrons of opposite charge and which satisfy $|y_1^* - y_2^*| < 1$. These requirements are chosen to enrich

* The parameters $\sigma_q$ and $\sigma'$ are the actual Lund model parameters. $\sigma_q$ is a factor of $\sqrt{2}$ larger than the quantity used in ref.[12].

the sample with pairs of particles which are adjacent in rank [18]. The quantity used to estimate $\sigma_q$ is the mean of the $\delta q$ distribution which is found to be

$$< \delta q >= 0.539 \pm 0.001 \pm 0.020 \text{ GeV}$$

where the first error is statistical and the second systematic[9].

In order to study the effect of $k_T$ on the event axis, a four vector $P$ was formed from summing the energy and momenta of all charged hadrons having $x_F < 0$, thus

$$P = (E, \underline{P}) = \left( \sum_i E_i \ , \ \sum_i \underline{p}_i \right)$$

The direction of $\underline{P}$ is taken as an estimate of the event axis. A plot of $< P_T >$ against $f$ is constructed, where $P_T$ is the component of $\underline{P}$ transverse to the virtual photon axis and $f = 2E/W$ is the fraction of the available centre of mass energy observed as charged particles. This is shown in fig.3. The value of $< P_T >$ at $f = 1$ is taken as an estimate of the value which would be obtained if no energy were lost in the form of undetected neutral particles. A linear fit to the points shown in fig.3 gives

$$< P_T(f = 1) >= 0.643 \pm 0.009 \pm 0.014 \text{ GeV}$$

The measured values of $< \delta q >$ and $< P_T(f = 1) >$ are shown in fig. 4, together with the values expected from the Lund model for different values of $\sigma_q$ and $\sigma'$. The error bars for the data include both statistical and systematic errors (added in quadrature) and the Lund model values are drawn as contours for constant values of $\sigma_q$ and $\sigma'$. Using a linear interpolation between the contours drawn on fig. 4, the following values are obtained

$$\sigma_q = 0.410 \pm 0.002 \pm 0.020 \text{ GeV}$$
$$\sigma' = 0.29^{+0.05+0.14}_{-0.07-0.18} \text{ GeV}$$

where the first error is statistical and the second systematic.

## 5. Comparison of $\mu p$ and $e^+e^-$ final states.

### 5.1 Scope of the comparison

One of the basic assumptions of the standard quark parton model is that the fragmentation of a given quark does not depend on the process by which the quark was excited. In this case the spectrum of hadrons is determined solely by the energy and flavour of the fragmenting quark. In this section the properties of the final state hadrons in $\mu p$ and $e^+e^-$ are compared in order to investigate whether this assumption is valid.

In the comparison of hadron production from deep inelastic $\mu p$ scattering and $e^+e^-$ annihilation, the $e^+e^-$ results were taken from the TASSO experiment [19]. In order that this comparison is meaningful the distributions presented have been corrected to correspond to distributions in which the hadrons from the decays of $K^\circ_S$, $\Lambda$ and $\bar{\Lambda}$ particles are included as primary hadrons, as is the

case for $e^+e^-$ interactions. In addition to the cuts described in section 2, the following cuts are made in order to ensure that the selection for the $\mu p$ event sample is as close as possible to that for $e^+e^-$. It is required that each event has a charged multiplicity of at least four. This selection is made so that the sphericity and thrust axes can be determined meaningfully. For the comparison of hadron properties as a function of $W$, $\mu p$ data upto $W = 20$ GeV are used. For the comparison of the $e^+e^-$ data at $W = 14$ GeV, it is demanded for the $\mu p$ data that $10 < W < 18$ GeV, which gives events with a mean $W$ value of 14.2 GeV.

For the analysis described in ref.[19] the data were corrected so that the distributions obtained correspond to those that would have been obtained if all charged and neutral particles were used to determine the event axis. The $\mu p$ results presented in section 5.2 have been obtained using charged particles only. When the comparison with the data for $e^+e^-$ annihilation is made (in section 5.3), the $\mu p$ data are corrected to correspond to distributions in which charged and neutral ($\pi^\circ$, $K^\circ_L$, $n$ and $\bar{n}$) particles have been used to determine the jet axis.

Before comparing the properties of the hadronic final states of $e^+e^-$ and $\mu p$ scattering, it is instructive to compare hadronic distributions referred to the different event axes (virtual photon, sphericity, and thrust). This study gives a quantitative assessment of the effect that the choice of event axis has on the hadronic distributions.

### 5.2 Comparison of event axes in $\mu p$ interactions

The $p_T^2$ distributions of hadrons with respect to the sphericity and thrust axes are compared to that with respect to the virtual photon ($\gamma_V$) axis in fig.5a and 5b respectively. The sphericity and thrust axes are calculated using all charged hadrons in the event. The distributions shown in fig.5 are different in shape. Since the sphericity axis is the axis for which $\sum p_T^2$ is a minimum, the corresponding $p_T^2$ distribution is shifted to smaller values of $p_T^2$. As a result, the $p_T^2$ distribution with respect to the sphericity axis is larger in the first bin and thereafter steeper than that with respect to the virtual photon axis. The thrust axis is the axis for which $\sum |p_L|$ is a maximum, so the $p_T^2$ with respect to the thrust axis must be smaller than that with respect to the $\gamma_V$ axis. The result is that the $p_T^2$ distribution with respect to the thrust axis is shifted to smaller $p_T^2$, in a way similar to that for the sphericity axis. The effect is, however, less pronounced than for the sphericity axis.

The longitudinal $x_F$ and $y^*$ distributions of hadrons with respect to the various axes are shown in fig.6. The distributions are rather similar, however some points are worthy of comment. The $x_F$ distribution with respect to the sphericity axis appears to be similar to that with respect to the $\gamma_V$ axis for all $x_F$. However, when plotted as a function of the cms rapidity $y^*$ (fig. 6c) some differences between the $\gamma_\nu$ and sphericity axes become apparent. The $y^*$ distribution with respect to the sphericity axis is smaller in the central bins, but extends to larger values of $| y^* |$. Furthermore, it is slightly skewed to positive $y^*$. These graphs show how the minimisation of $\sum p_T^2$ tends to increase the component of a hadron's momentum parallel to the event axis. The effect is to

populate the wings of the $x_F$ or $y^*$ distribution at the expense of the central bins. The skewed sphericity distribution is a reflection of the fact that there is more transverse momentum in the forward hemisphere of the centre of mass system than in the backward hemisphere.

In figs. 6b and d the longitudinal distributions with respect to the thrust and $\gamma_V$ axes are compared. The central bins of the $x_F$ distribution are lower with respect to the thrust axis than with respect to the $\gamma_V$ axis. The effect is more pronounced than for the sphericity axis, as indicated by the large dip in the central region in the rapidity distribution (see fig. 6d). The thrust axis is the axis for which $\sum |p_L|$ is a maximum. Thus, when particle momenta are referred to the thrust axis the wings of the distributions of $x_F$ and $y^*$ are populated at the expense of the central bins. The close agreement of the $y^*$ distributions for $y^* < -1.5$ in fig. 6d, indicates that the thrust axis is largely determined by the more pencil-like jet in the target fragmentation region and that the thrust axis is close to $\gamma_V$.

In fig. 7a a comparison of the average transverse momentum $< p_T^2 >$ of hadrons versus $x_F$ (the seagull plot), with respect to the sphericity and $\gamma_V$ axes is shown. Although the differential distributions presented in fig.6 are rather similar, the seagull plot with respect to the sphericity axis is very different to that relative to the $\gamma_V$ axis. The values of $< p_T^2 >$ are symmetric around $x_F = 0$ for the sphericity axis, but asymmetric for the $\gamma_V$ axis. Further, the values of $< p_T^2 >$ with respect to the sphericity axis are always lower than the values relative to the $\gamma_V$ axis. This is expected from the definition of the sphericity axis.

The seagull plot with respect to the thrust and $\gamma_V$ axes are compared in fig. 7b and it can be seen that for the thrust axis the values are symmetric. The two distributions are compatible for $x_F < 0$ but the $< p_T^2 >$ values are larger for the $\gamma_\nu$ axis than for the thrust axis for $x_F > 0$. The thrust axis is closer to the $\gamma_\nu$ axis than is the sphericity axis.

Thus the major difference observed in the properties of final state hadrons when referred to hadronic event axes rather than the $\gamma_V$ axis is the loss of the asymmetry in the seagull plot. In terms of the phenomenology of the Lund model a large contribution to the asymmetry has been shown [6] to be caused by soft gluon radiation. One may conclude that the reconstruction of the hadronic event axis effectively averages out the effects of soft gluon radiation. Hence the transverse momentum distributions with respect to the axes determined using the hadrons themselves are less sensitive to the underlying physical effects.

### 5.3 Comparison of $\mu p$ with $e^+e^-$

In this section a comparison is made between the hadrons produced in deep inelastic $\mu p$ scattering and those produced in $e^+e^-$ annihilation [19]. The inclusive differential distributions are compared at a centre of mass energy of 14 GeV for the $e^+e^-$ data and 14.2 GeV for the $\mu p$ data. In making such a comparison it should be borne in mind that the average multiplicity in $e^+e^-$ annihilation at 14 GeV is $\sim 9$, while for the deep inelastic $\mu p$ scattering data presented here it is $\sim 7$.

The comparison is made only for hadrons produced in the fragmentation

region of the struck quark, i.e. for hadrons with $x_F > 0$ but the sphericity and thrust axes are determined using hadrons in both hemispheres. In order that a direct comparison may be made, the differential cross-sections for hadron production in $e^+e^-$ annihilation have been divided by two so that the latter refer to a single jet. The comparison is made for distributions with respect to the sphericity axis unless stated to the contrary. All differential distributions are normalised to the total number of events satisfying the cuts described above.

The $p_T^2$ distributions of the final state hadrons transverse to the event axis are compared in fig.8a. The agreement between the two data sets is, in general, good. For very small values of $p_T^2$ ($p_T^2 < 0.1$ GeV$^2$) the $p_T^2$ distribution for $e^+e^-$ is, in fact, larger than that for $\mu p$ scattering. The two distributions are very similar for $p_T^2$ in the range $0.1 < p_T^2 < 0.4$ GeV$^2$. For $p_T^2 > 0.4$ GeV$^2$ the $e^+e^-$ data lie above those from $\mu p$ scattering. The $p_T^2$ spectrum of hadrons produced in $e^+e^-$ annihilation tends to be somewhat harder than that for $\mu p$ scattering as can be seen from fig. 8b which shows $< p_T^2 >$ as a function of $W^2$. However, these differences are only of about the same size as the possible systematic errors on the data sets.

The longitudinal distributions for $x_F$ are compared in fig. 9a. The $e^+e^-$ data lie somewhat above the $\mu p$ data in the first two or three bins, and the distribution for hadrons produced in $e^+e^-$ annihilation is slightly steeper than that for $\mu p$ scattering. The same effects are observed when the $y^*$ distributions are compared (fig.9b). There is a marked difference between the two distributions in the central bins. Care must be taken when considering the points at large values of $|y^*|$. It is important to remember that the $e^+e^-$ data shown in this figure were collected at a fixed value of $W$ ($= 14$ GeV), whereas the value of $W$ for the $\mu p$ data lies in the range $10 < W < 18$ GeV. The longitudinal momentum distributions are softer in $e^+e^-$ annihilation than in $\mu p$ scattering as a function of $W^2$ as can be seen from the plot of $< p_L >$ versus $W^2$ in fig.9c ($p_L$ is the momentum component parallel to the event axis).

The seagull plots, with respect to the sphericity and thrust axes, are shown in fig.10. The seagull plot with respect to the sphericity axis (fig.10a) shows that the hadrons from $e^+e^-$ annihilation have a somewhat harder $p_T^2$ distribution (i.e. a larger value of $< p_T^2 >$) for $x_F$ in the range $0.05 < x_F < 0.3$. A similar trend is observed in fig.10b where the seagull plots with respect to the thrust axis are compared. Here the $e^+e^-$ data have a harder $p_T^2$ distribution for $0.05 < x_F < 0.6$.

The distributions of sphericity $S$ and thrust $T$ are compared in fig. 11. For the $\mu p$ events all the charged hadrons in the event are used in computing the values of $S$ and $T$. The $\mu p$ events are less spherical (fig. 11a) and more thrusting (fig. 11b) than the $e^+e^-$ events. The average values of the sphericity ($< S >$) and thrust ($< T >$) as a function of $W^2$ are shown in fig. 12.

In conclusion, these studies indicate that hadrons produced in $e^+e^-$ annihilation have a softer longitudinal momentum spectrum, and a harder transverse momentum spectrum than the hadrons produced in the current jet of deep inelastic $\mu p$ scattering; $e^+e^-$ events are more spherical (less thrusting) than leptoproduction events. In general these differences are fairly small, and one may conclude that the parton model assumption of environmental independence is

reasonably well satisfied.

It is interesting to enquire into the origin of the differences observed. There are two main differences between the jets produced in $e^+e^-$ annihilation and the current jet in $\mu p$ scattering. Firstly, as discussed in section 1, the proportion of primary heavy quarks is larger in $e^+e^-$ annihilation than in $\mu p$ scattering, where the current jet is most likely to have been initiated by a $u$ quark. The second difference arises from the fact that in $e^+e^-$ annihilation there is a higher chance per event that a hard gluon will have been radiated since it can be produced from either the quark or antiquark, whereas in $\mu p$ scattering the diquark is assumed to act as a spectator. Both these effects may contribute to the observed differences. In addition, there is no analogue of the photon-gluon fusion process in $e^+e^-$ annihilation.

In order to separate these contributions Monte Carlo events were generated using the Lund model for $e^+e^-$ annihilations [20]. The solid curves in figs. 10 and 11 represent the predictions of the standard Lund model. The dashed lines are the result obtained from the model if only $u$ quark jets are generated. The dot-dashed lines represent the predictions of the Lund model where the effect of (hard) QCD corrections to the process $e^+e^- \rightarrow q\bar{q}$ have been neglected. Note that soft gluon emission, as parametrised in the Lund model, is included and that all quarks (i.e. $u$, $d$, $s$, $c$, $b$) are considered. The dotted curves represent the predictions of the Lund model where only $u$ quark jets are generated and the effects of hard QCD are excluded.

The seagull plot, obtained from $e^+e^-$ annihilation at 14 GeV, is well reproduced by the standard Lund model (see fig.10). The contribution from the decays of hadrons containing heavy quarks to the seagull plot is shown by the difference between the solid and dashed lines in figs. 10a and b. A reduction in $< p_T^2 >$ is seen for values of $x_F \lesssim 0.4$. The $< p_T^2 >$ is also reduced when hard QCD is ignored. This is shown by the difference between the dash-dotted and solid lines in figs. 10a and b. The seagull plot obtained from the model where only $u$ quark jets are generated and the hard QCD processes are ignored (dotted lines) lies close to the points obtained from this experiment. The differential sphericity and thrust distributions (fig. 11) show a similar behaviour. The curves from the Monte Carlo with no hard QCD and only $u$ quark jets lie closer to the $\mu p$ data than either of the other $e^+e^-$ models. Note that, in general, the standard Lund model for $e^+e^-$ annihilation reproduces the $e^+e^-$ data reasonably well. A similar conclusion holds for the $\mu p$ data, as discussed in ref. [6].

A large fraction of the energy of the target jet in $\mu p$ scattering is taken by the recoiling baryon, mostly a proton or a neutron with roughly equal probability. This particle is most likely to be found at large negative $x_F$. One way to investigate the effect that this particle has on the determination of the jet axis is to remove protons and neutrons for which $x_F < 0$ from the particle sample. When this is done (using the Monte Carlo) it is found that the average value of the sphericity increases (from $< S > \approx 0.11$ to $< S > \approx 0.17$), and the average value of the thrust decreases (from $< T > \approx 0.89$ to $< T > \approx 0.86$). In $e^+e^-$ annihilation at 14 GeV, the average values of sphericity and thrust are found to

be [19]:

$$< S > = 0.213 \pm 0.004,$$
$$< T > = 0.855 \pm 0.002.$$

Thus, when the recoiling baryon is removed from the particle sample the distributions of $S$ and $T$ become more similar to their $e^+e^-$ counterparts. There is little change in the seagull plot referred to the sphericity axis, whereas the seagull plot referred to the thrust axis changes significantly. Nonetheless the observed differences between the properties of hadrons produced in deep inelastic $\mu p$ scattering and those obtained from $e^+e^-$ annihilations can not be attributed solely to the presence of a baryon in the target jet in deep inelastic scattering.

To conclude, it has been shown that:

i) The parton model assumption of environmental independence is reasonably well satisfied.

ii) The differences between the properties of hadrons produced in deep inelastic $\mu p$ scattering and $e^+e^-$ annihilation have been shown to be attributable, at least in part, to:
   a. The production of heavy quarks in $e^+e^-$ annihilation.
   b. The fact that the QCD corrections to the parton model predictions are different for $e^+e^-$ annihilation and $\mu p$ scattering.
   c. The fact that the thrust axis in $\mu p$ scattering is affected by a fast particle (the recoiling baryon) from the target remnant.

## 6. Comparison of the $p_T$ distributions in $\mu p$ and $K^+p$ interactions

In this section a comparison of the $p_T^2$ distribution measured in $K^+p$ interactions at $W = 11.5$ GeV [21] with that in $\mu p$ interactions is made. Inelastic hadronic interactions are envisaged to be mainly the result of soft and possibly multiple collisions at the parton level. Hence the $p_T^2$ distributions are expected to arise primarily from the fragmentation process. A small fraction of the collisions may involve a relatively hard parton-parton collision giving a high $p_T^2$ tail to the $p_T^2$ distribution, measured relative to the beam axis However, this tail is expected to arise from a smaller fraction of events than that in deep inelastic $\mu p$ collisions, where the interaction is primarily that of a single hard $\gamma_V$-quark interaction. It is of interest therefore, where data is available, to compare the $p_T^2$ distributions in these interactions.

In the analysis of the 70 GeV $K^+p$ data [21], diffractive events are removed. A diffractive event is defined as one with at least one track satisfying $|x_F| > 0.8$, and these events constitute about 18% of the sample. For the remaining non-diffractive events it is required that $n_{ch} \geq 4$. It was required that the $\mu p$ events for this comparison had $n_{ch} \geq 4$ and $90 < W^2 < 170$ GeV$^2$, to be compared with $W^2 = 132$ GeV$^2$ for the $K^+p$ sample. Fig.13 shows a comparison of the average transverse momentum $< p_T^2 >$ as a function of $x_F$, where $p_T$ is defined with respect to the thrust axis. It can be seen that the distributions are rather similar in shape with the $K^+p$ interactions having a somewhat larger value of $< p_T^2 >$ in the range $0.1 < |x_F| < 0.5$, both forwards and backwards. At large $|x_F|(\gtrsim 0.5)$ the $\mu p$ errors become rather large but the results are compatible.

## 7. Summary and Conclusions

Many features of the hadron final states in deep inelastic $\mu p$ scattering can be well reproduced by the Lund model. Estimates of two parameters in this model which influence the transverse momentum distributions of the final state hadrons have yielded the values

$$\sigma_q = 0.410 \pm 0.002 \pm 0.020 \text{ GeV}$$
$$\sigma' = 0.29^{+0.05+0.14}_{-0.07-0.18} \text{ GeV}$$

where $\sigma_q$ and $\sigma'$ describe the fragmentation transverse momentum and intrinsic transverse momentum of the struck quark respectively. The first error is statistical, the second systematic.

A comparison has been made of the longitudinal and transverse momentum distributions of hadrons in $\mu p$ interactions with respect to the virtual photon, sphericity and thrust axes. The longitudinal distributions of $x_F$ and $y^*$ are rather similar with respect to the three axes, but the values in the central $x_F$ (or $y^*$) bins with respect to the sphericity and thrust axes are somewhat lower than those with respect to $\gamma_V$, whereas the opposite is true at large $|x_F|$. The $< p_T^2 >$ values with respect to the sphericity and thrust axes are lower in the forward hemisphere than those with respect to $\gamma_V$. The values of $< p_T^2 >$ in the forward hemisphere are much larger than those in the backward hemisphere when measured with respect to the $\gamma_V$ axis. This effect, which may be due to soft gluon radiation, is largely washed out when the hadrons are used to determine the jet axes. The data on $< p_T^2 >$ versus $x_F$, with respect to the sphericity and thrust axes, are symmetric.

The comparison of the $\mu p$ data with $e^+e^-$ data at a similar centre of mass energy shows that, whereas the trends with $W$ in both cases are the same, there are small but significant differences in both the longitudinal and transverse momentum properties. The hadrons in $e^+e^-$ have a softer longitudinal momentum spectrum, and a harder transverse momentum spectrum than the hadrons produced in the current jet of $\mu p$ scattering. These differences, at least in part, are attributable to the higher production of heavy quarks and the larger QCD corrections to the parton model in $e^+e^-$ annihilation, and to the influence of the more pencil like target remnant jet in $\mu p$ scattering, which significantly effects the determination of the thrust axis. These differences are, however, relatively small and the parton model assumption of environmental independence is reasonably well satisfied.

The similarity of the $p_T^2$ distributions in $K^+p$ and $\mu p$ interactions at a value of $W \sim 10$ GeV shows that non-perturbative fragmentation effects are probably dominant. However at the highest accessible values of $W$ ($\sim 20$ GeV) in $\mu p$ interactions there is a significant growth in the high $p_T^2$ tail, consistent with hard QCD effects [22].

## Acknowledgements

We would like to thank all the people in the various laboratories who have contributed to the construction, operation and analysis of this experiment. The support of the CERN staff in operating the SPS, muon beam and computer facilities is gratefully acknowledged. We also thank P. Dauncey for a useful discussion.

## References


[1] E.M.C., J.P.Albanese *et al.*, *Phys. Lett.* **144B**, 302 (1984)
[2] E.M.C., A.Arvidson *et al.*, *Nucl. Phys.* **B246**, 381 (1984)
[3] E.M.C., M.Arneodo *et al.*, *Phys. Lett.* **150B**, 458 (1985)
[4] J.Bjorken and S.Brodsky, *Phys. Rev.* **D1**, 1416 (1970)
[5] S.Brandt *et al.*, *Phys. Lett.* **12**, 57 (1964); E.Farhi, *Phys. Rev. Lett.* **39**, 1587 (1977)
[6] E.M.C., M.Arneodo *et al.*, *Phys. Lett.* **149B**, 415 (1984)
[7] G.Ingelman *et al.*, *Nucl. Phys.* **B206**, 239 (1982); B.Andersson *et al.*, *Phys. Rep.* **97**, 31 (1983)
[8] E.M.C., J.P.Albanese *et al.*, *N.I.M.* **212**, 111 (1983)
[9] K.Long. A Study of the Hadrons Produced in Deep Inelastic Muon Proton Scattering, D.Phil Thesis, University of Oxford 1984; RAL T 001.
[10] E.M.C., J.J.Aubert *et al.*, *Phys. Lett.* **133B**, 370 (1983)
[11] E.M.C., M.Arneodo *et al.*, *Phys. Lett.* **145B**, 156 (1984)
[12] E.M.C., J.J.Aubert *et al.*, *Phys. Lett.* **100B**, 433 (1981)
[13] E.M.C., J.J.Aubert *et al.*, *Phys. lett.* **119B**, 233 (1982)
[14] JADE, W.Bartel *et al.*, *Phys. Lett.* **145B**, 441 (1984)
[15] TPC, H.Aihara *et al.*, *Phys. Rev. Lett.* **53**, 2378 (1984)
[16] TASSO, M.Althoff *et al.*, *Z. Phys.* *C***26**, 157 (1984); *Z. Phys.* *C***27** (1985)
[17] T.Meyer, *Z. Phys.* *C***12**, 77 (1982)
[18] E.M.C., M.Arneodo *et al.*, *Z. Phys.* *C***31**, 333 (1986)
J.Krüger, Ph.D. Thesis, Univ. of Wupertal, *WU B-DI* **85-4**.
[19] TASSO, M.Althoff *et al.*, *Z. Phys.* *C***22**, 307 (1984)
[20] T.Sjöstrand, *Comp. Phys. Comm.* **28**, 229 (1983)
[21] M.Barth *et al.*, *Nucl. Phys.* **B192**, 289 (1981)
[22] E.M.C., J.J.Aubert *et al.*, *Phys. Lett.* **95B**, 306 (1980)

## Figure Captions

Fig.1. The simplest parton final states describing the reaction $e^+e^- \rightarrow$ hadrons. The leading order QCD process is shown in a), whereas the $0(\alpha_s)$ corrections involving external gluon lines are shown in b) and c).

Fig.2. The simplest parton final states describing the reaction $\mu^+p \rightarrow \mu^+ +$ hadrons. The leading order QCD process is shown in a) for the case of scattering off a $u$ valence quark. The $0(\alpha_s)$ diagrams leading to the emission of a hard gluon are shown in b) and c). The diagrams for the photon-gluon fusion process are shown in d) and e).

Fig.3. Average value of $P_T$ as a function of $f$ (see text), together with a linear fit and the result of extrapolating to $f = 1$. The inner error bars show the statistical errors.

Fig.4. Plot of $< \delta q >$ versus $< P_T(f = 1) >$. The Lund model predictions for contours of constant values of $\sigma_q$ and $\sigma'$ (in GeV) are shown together with the experimentally measured values. The errors include both statistical and systematic effects.

Fig.5. Distributions of $p_T^2$ of hadrons in $\mu p$ scattering with respect to a) virtual photon and sphericity axes and b) virtual photon and thrust axes.

Fig.6. Longitudinal distributions of $x_F$ with respect to a) $\gamma_V$ and sphericity, b) $\gamma_V$ and thrust, and of $y^*$ with respect to c) $\gamma_V$ and sphericity, d) $\gamma_V$ and thrust. The distributions are for hadrons in $\mu p$ scattering.

Fig.7. Seagull plot for $\mu p$ scattering; $< p_T^2 >$ as a function of $x_F$, with respect to a) $\gamma_V$ and sphericity axes, b) $\gamma_V$ and thrust axes.

Fig.8. Transverse momentum of hadrons from EMC ($\mu p$) and TASSO ($e^+e^-$). a) $p_T^2$ distribution and b) $< p_T^2 >$ against $W^2$. $p_T$ is defined with respect to the sphericity axis.

Fig.9. Longitudinal momentum of hadrons from EMC ($\mu p$) and TASSO ($e^+e^-$). a) $x_F$ distribution, b) $y^*$ distribution and c) $< p_L >$ against $W^2$.

Fig.10. Average transverse momentum $< p_T^2 >$ of hadrons as a function of $x_F$ for EMC ($\mu p$) and TASSO ($e^+e^-$), a) with respect to the sphericity axis and b) with respect to the thrust axis. The solid lines show the prediction of the standard Lund model for $e^+e^-$ annihilation, the dashed curves were obtained using only $u$ quark jets. The dot-dashed curve shows the predictions of the Lund model where hard QCD effects are ignored, and the dotted line was obtained using only $u$ quark jets and neglecting hard QCD effects.

Fig.11. Distributions of a) sphericity and b) thrust from EMC ($\mu p$) and TASSO ($e^+e^-$). The curves are as in Fig.10.

Fig.12. Mean values of a) sphericity $< S >$ and b) thrust $< T >$, as a function of $W^2$, from EMC ($\mu p$) and TASSO ($e^+e^-$).

Fig.13. Average transverse momentum $< p_T^2 >$ versus $x_F$ for hadrons produced in $K^+p$ interactions [21] and in $\mu p$ interactions. The transverse momentum is measured with respect to the thrust axis.

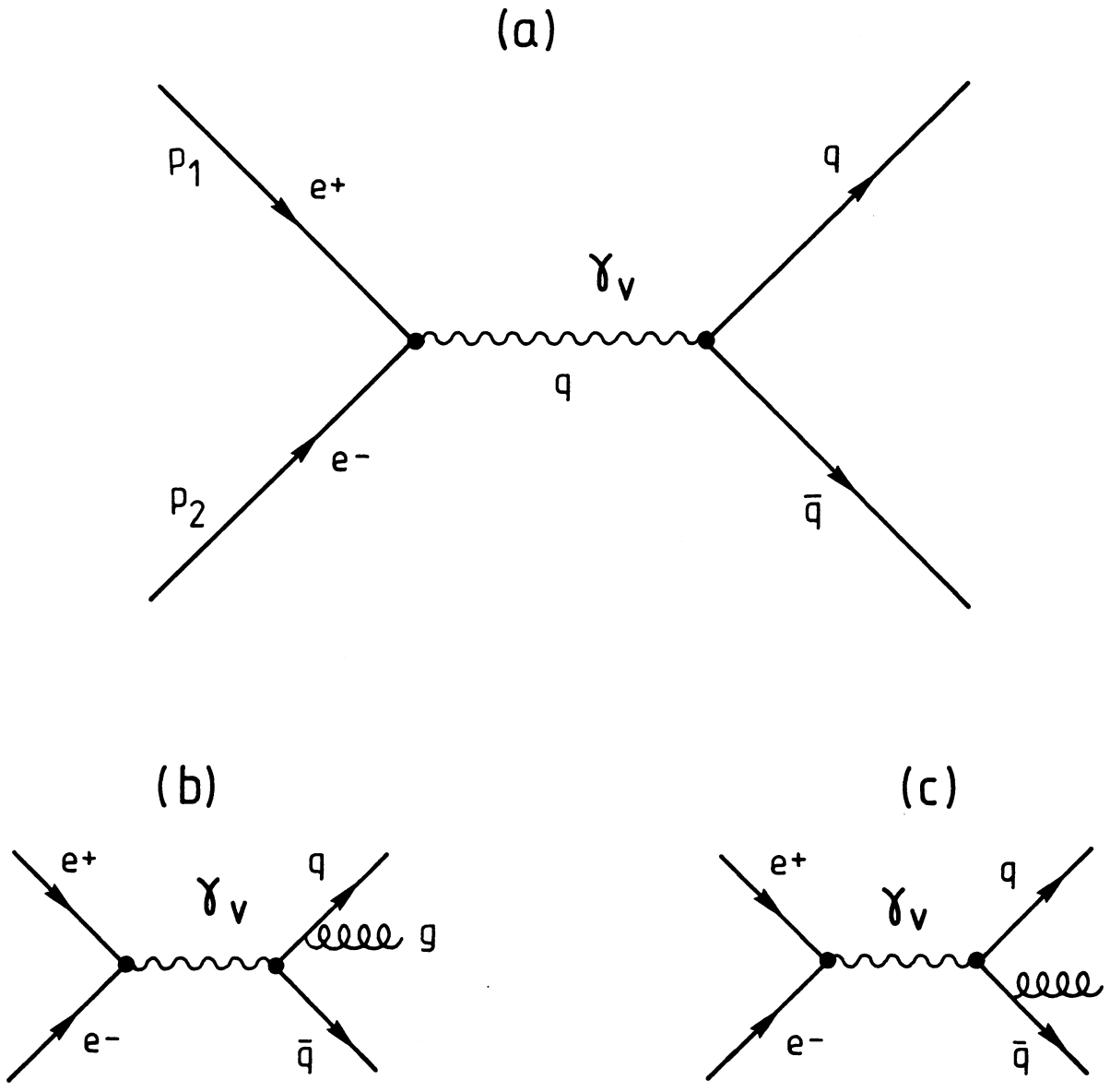


FIG. 1.

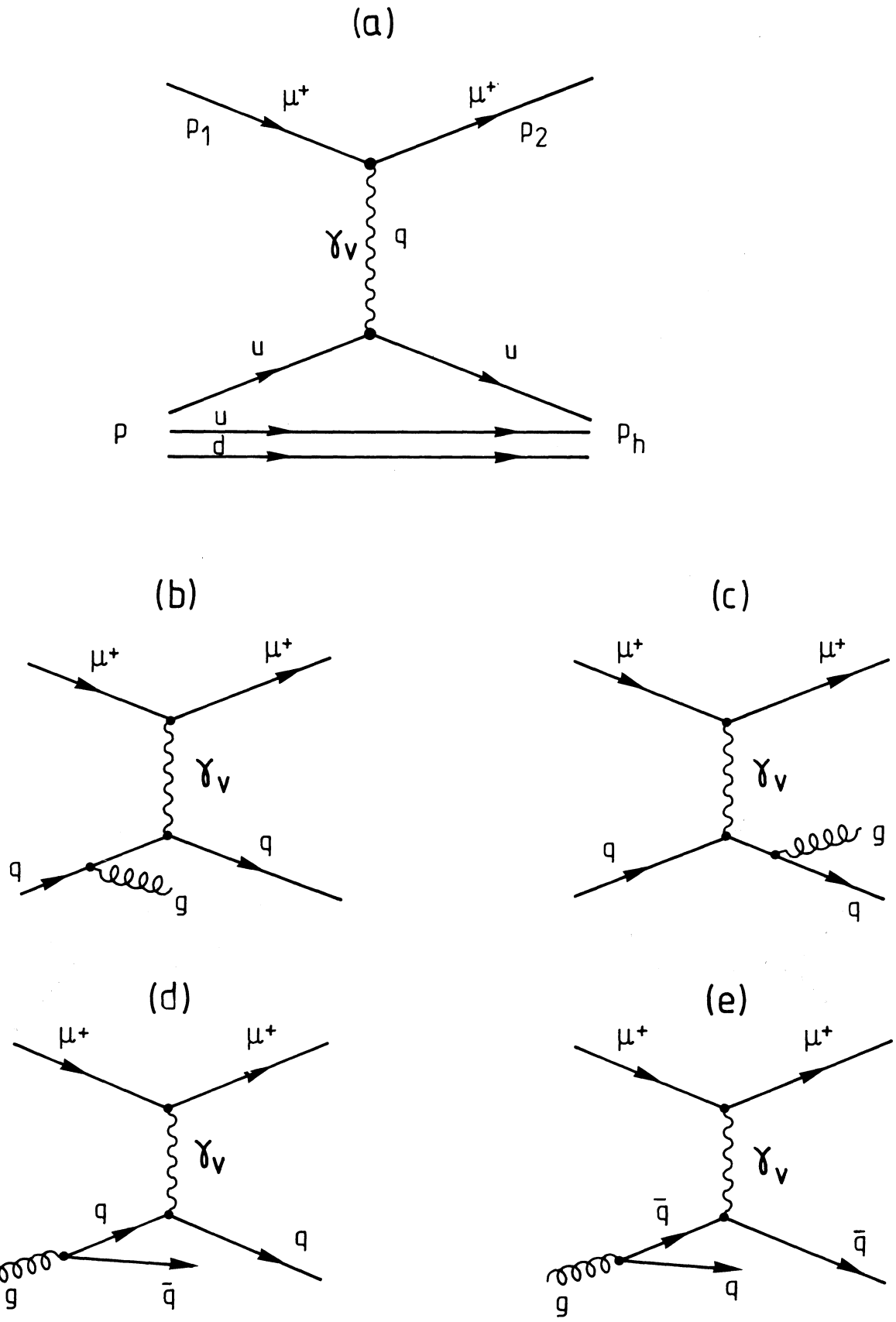
(a)
μ+
μ+
p1
p2
γv
q
u
u
p
u
d
ph
(b)
μ+
μ+
γv
q
q
g
(c)
μ+
μ+
γv
q
g
q
(d)
μ+
μ+
γv
q
q
g
q̄
(e)
μ+
μ+
γv
q̄
q̄
g
q

FIG. 2.

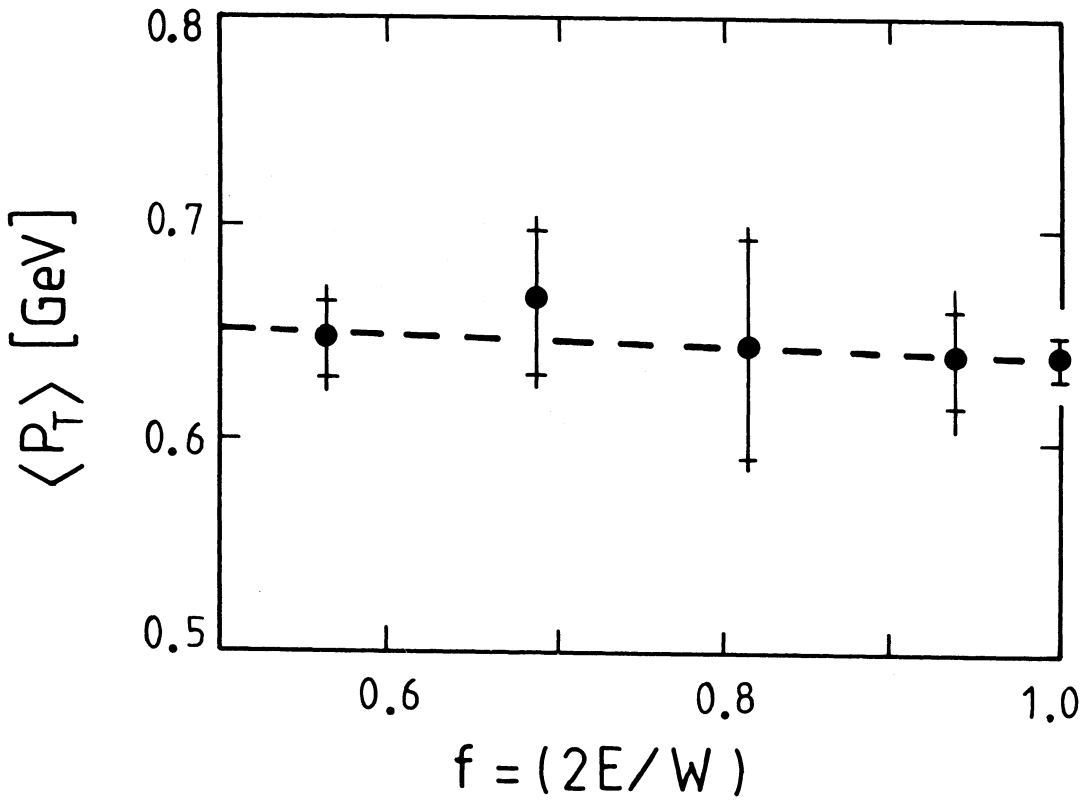


FIG. 3.

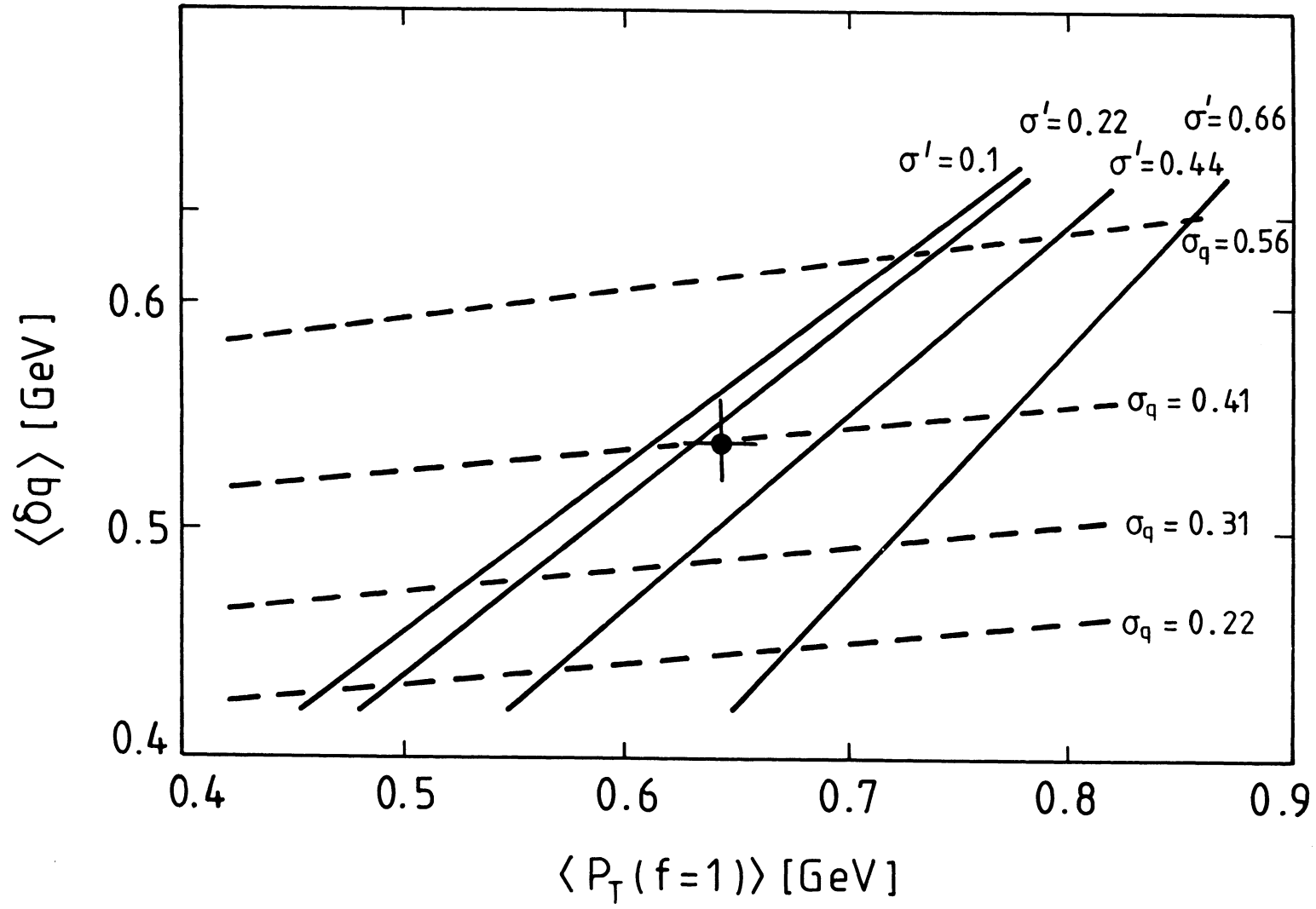
σ'=0.1
σ'=0.22
σ'=0.44
σ'=0.66
σq=0.56
σq = 0.41
σq = 0.31
σq = 0.22
0.4
0.5
0.6
0.7
0.8
0.9
⟨δq⟩ [GeV]
⟨ PT ( f=1 )⟩ [GeV]

FIG. 4.

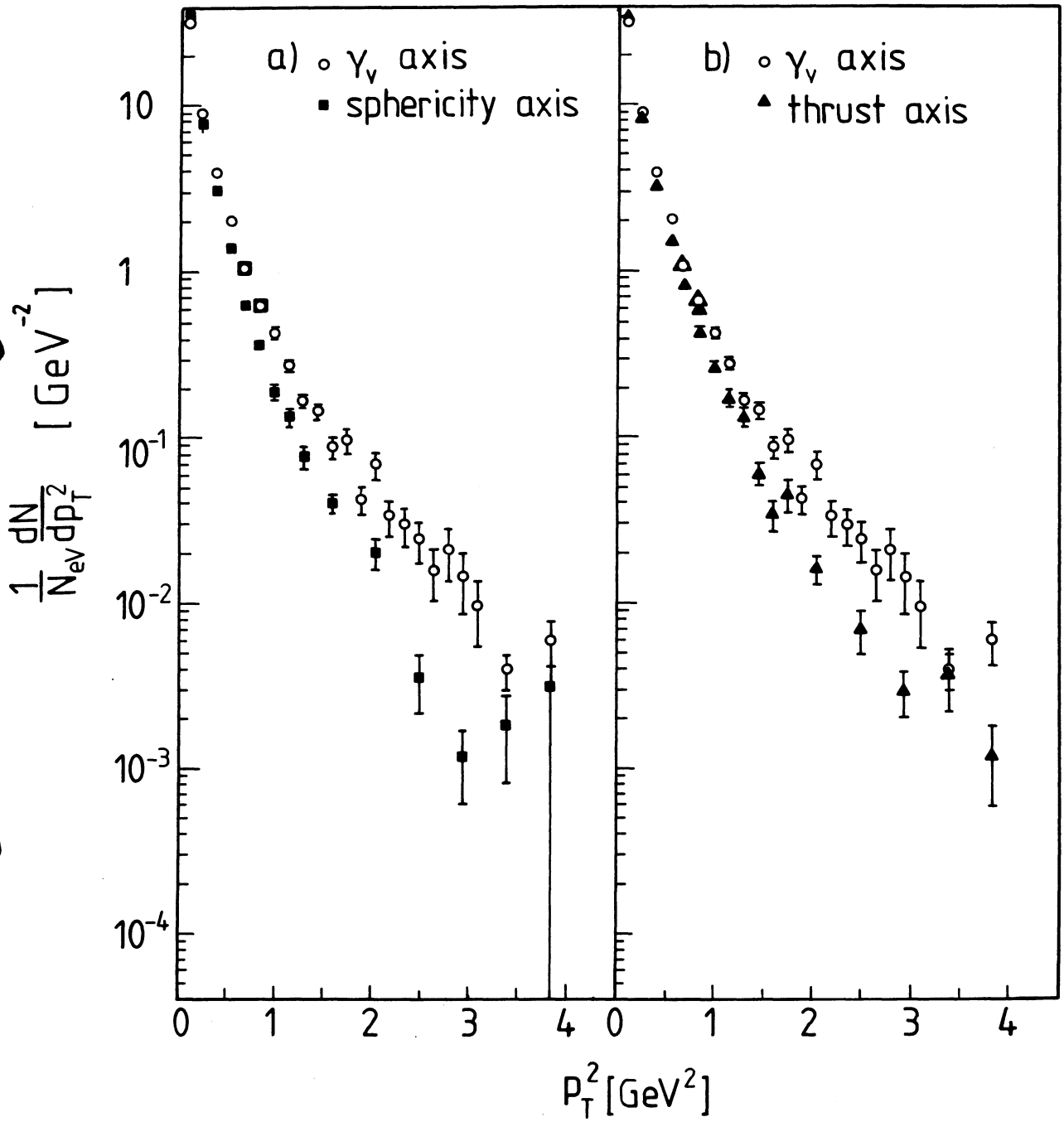
a) ○ $\gamma_v$ axis
■ sphericity axis
b) ○ $\gamma_v$ axis
▲ thrust axis
$\frac{1}{N_{ev}}\frac{dN}{dp_T^2}$ [GeV$^{-2}$]
10
1
$10^{-1}$
$10^{-2}$
$10^{-3}$
$10^{-4}$
0
1
2
3
4
$P_T^2$ [GeV$^2$]

FIG. 5.

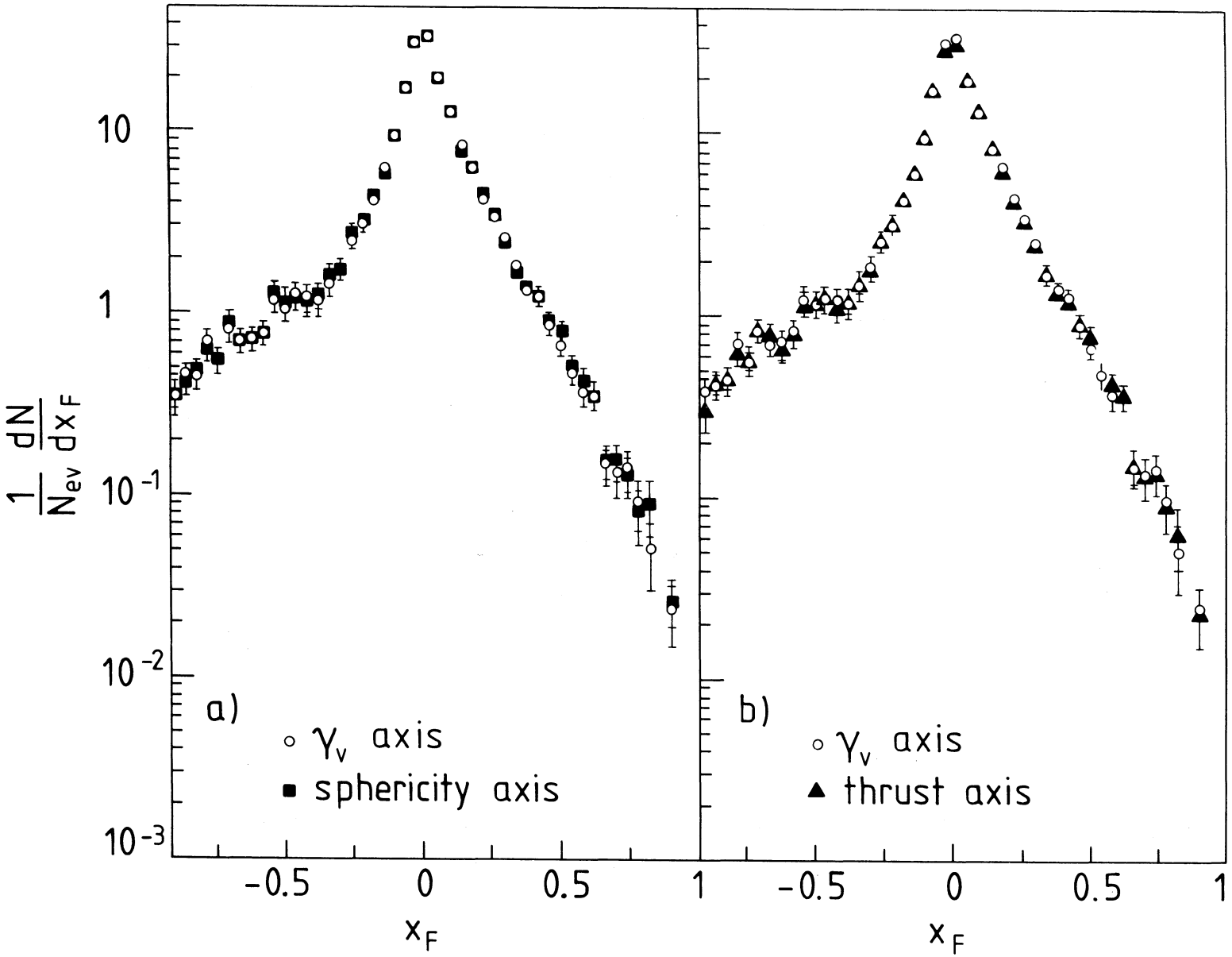
$\frac{1}{N_{ev}}\frac{dN}{dx_F}$
10
1
$10^{-1}$
$10^{-2}$
$10^{-3}$
a)
$\circ\ \gamma_v$ axis
■ sphericity axis
b)
$\circ\ \gamma_v$ axis
▲ thrust axis
-0.5
0
0.5
1
$x_F$

FIG. 6 a,b.

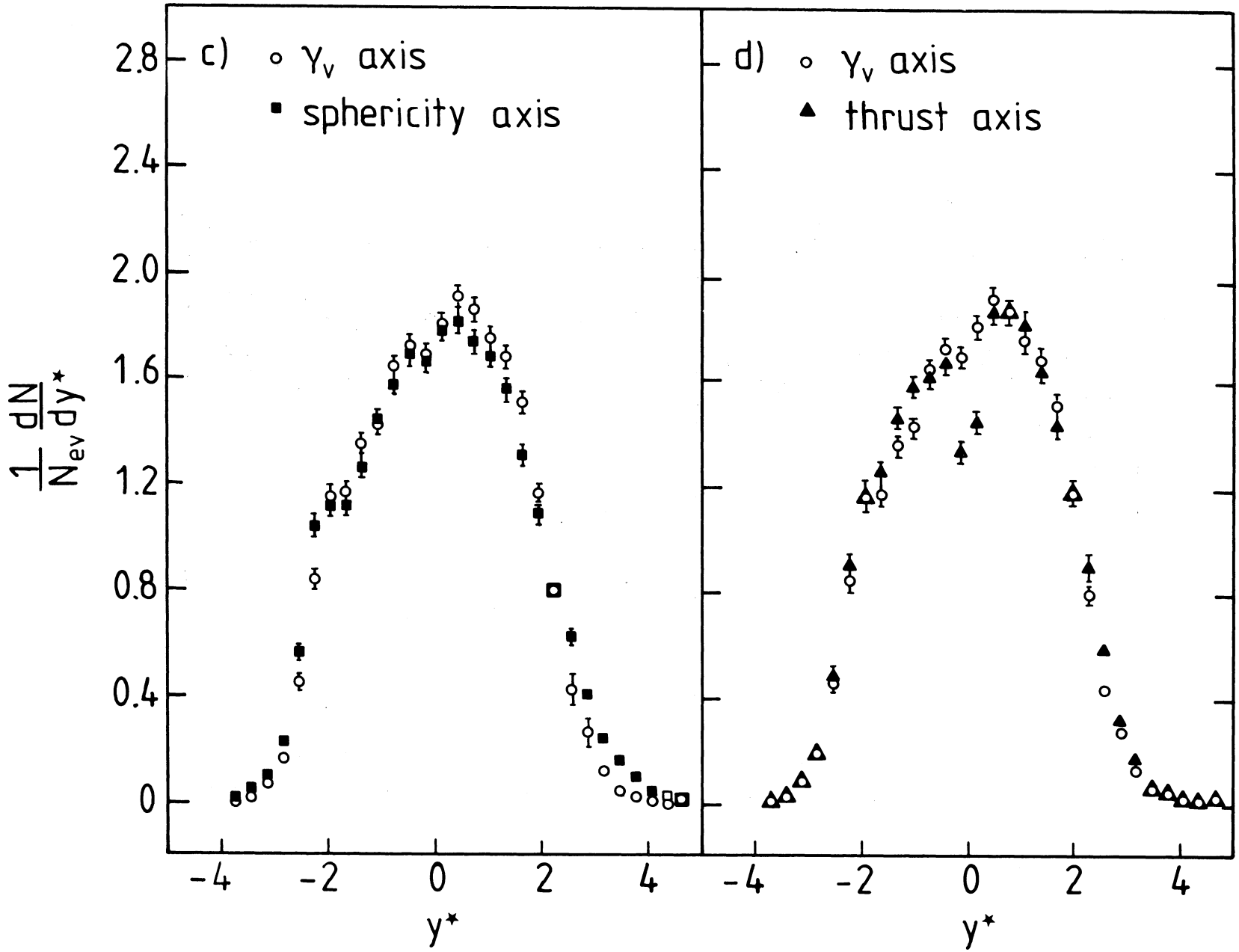
c)
$\gamma_v$ axis
sphericity axis
d)
$\gamma_v$ axis
thrust axis
$\frac{1}{N_{ev}} \frac{dN}{dy^*}$
2.8
2.4
2.0
1.6
1.2
0.8
0.4
0
-4
-2
0
2
4
$y^*$

FIG. 6 c,d.

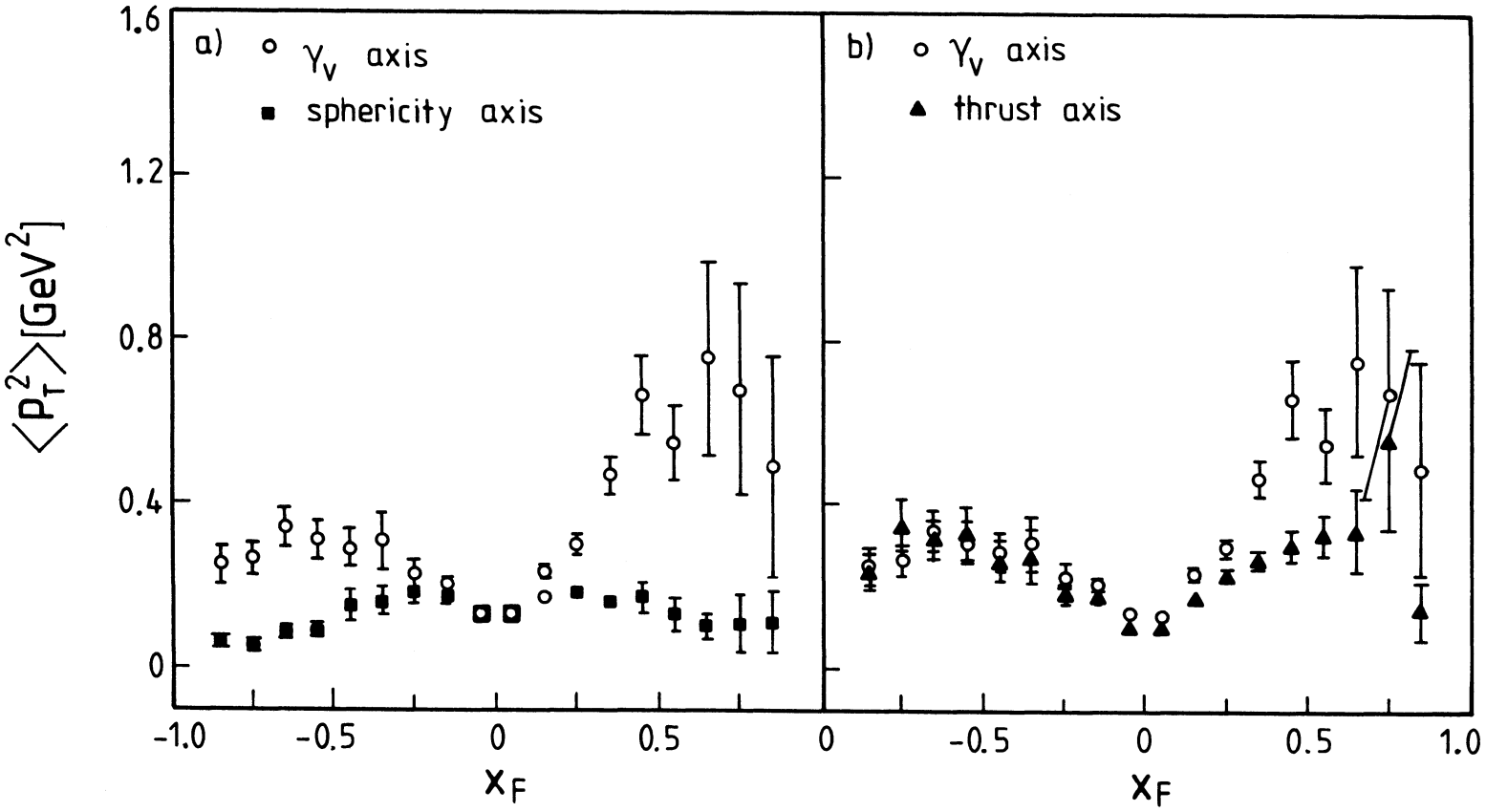
a)
$\gamma_v$ axis
sphericity axis
b)
$\gamma_v$ axis
thrust axis
$\langle p_T^2 \rangle$ [GeV$^2$]
1.6
1.2
0.8
0.4
0
-1.0
-0.5
0
0.5
1.0
$x_F$

FIG. 7.

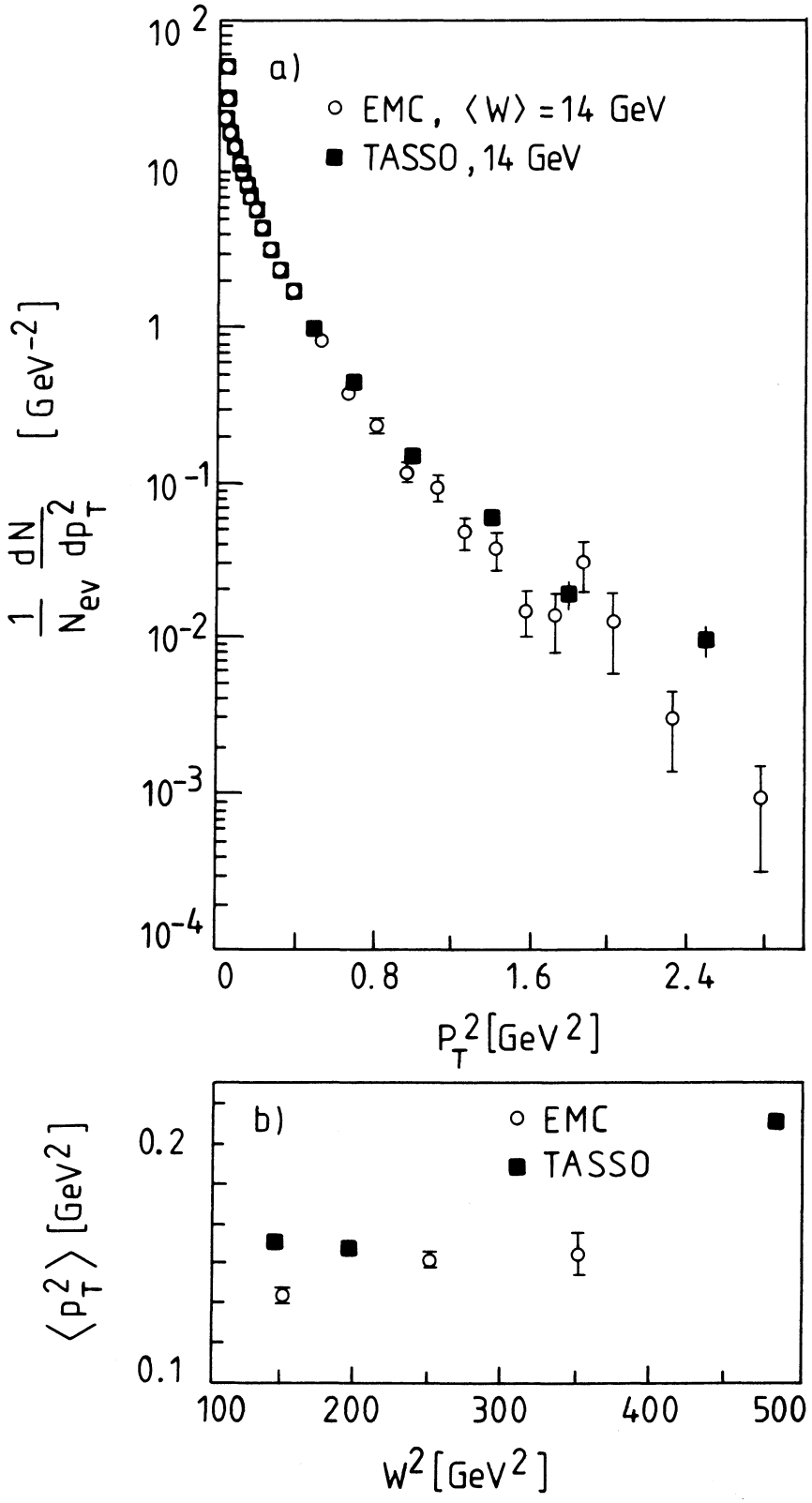
a)
EMC, ⟨W⟩ = 14 GeV
TASSO, 14 GeV
$\frac{1}{N_{ev}} \frac{dN}{dp_T^2}$ [GeV$^{-2}$]
$P_T^2$ [GeV$^2$]
b)
EMC
TASSO
$\langle p_T^2 \rangle$ [GeV$^2$]
$W^2$ [GeV$^2$]

FIG. 8.

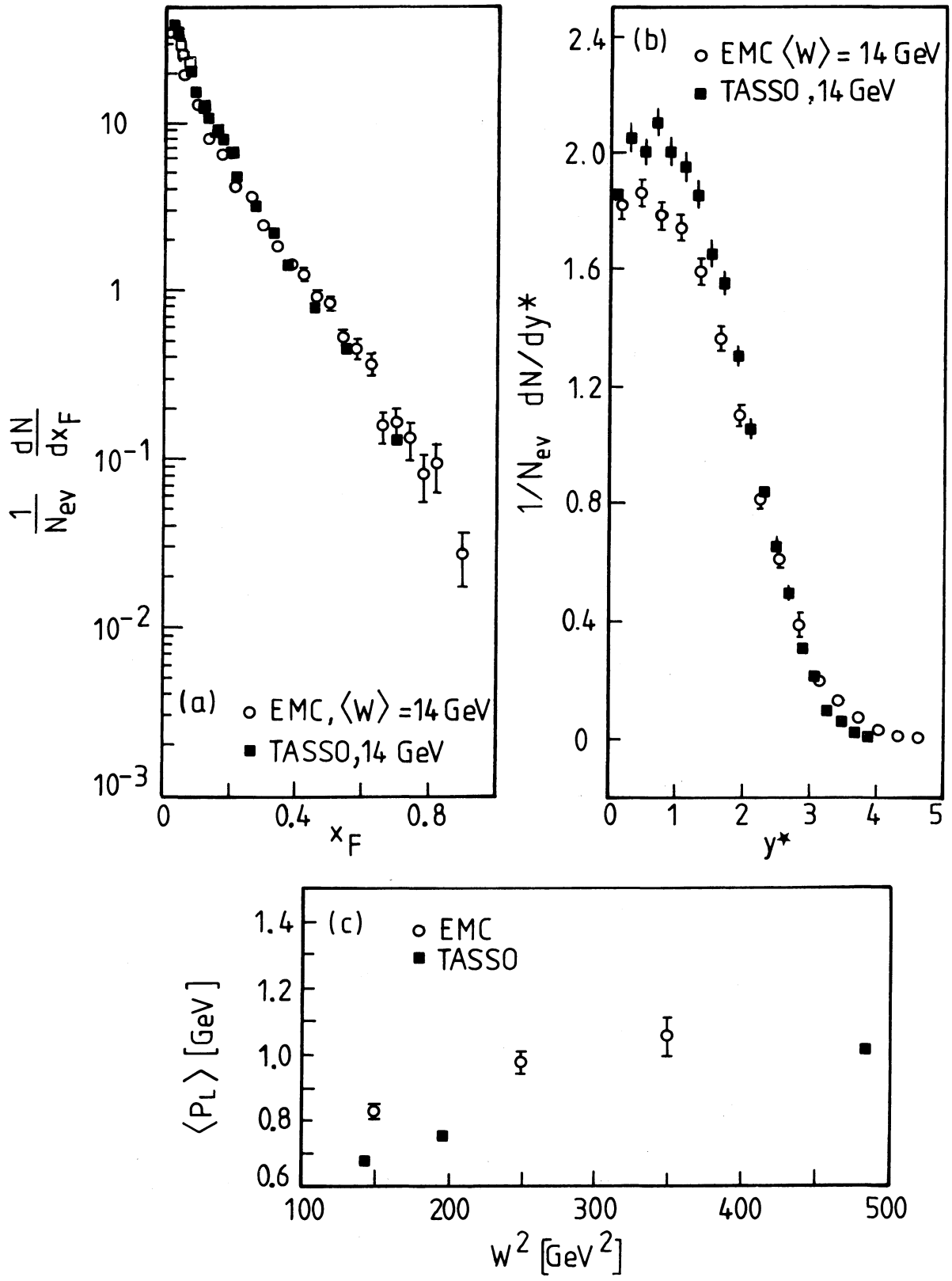
(a)
EMC, ⟨W⟩ =14 GeV
TASSO,14 GeV
$\frac{1}{N_{ev}} \frac{dN}{dx_F}$
$x_F$
(b)
EMC ⟨W⟩ = 14 GeV
TASSO ,14 GeV
$1/N_{ev}\ dN/dy^*$
$y^*$
(c)
EMC
TASSO
$\langle P_L \rangle$ [GeV]
$W^2$ [GeV$^2$]

FIG. 9.

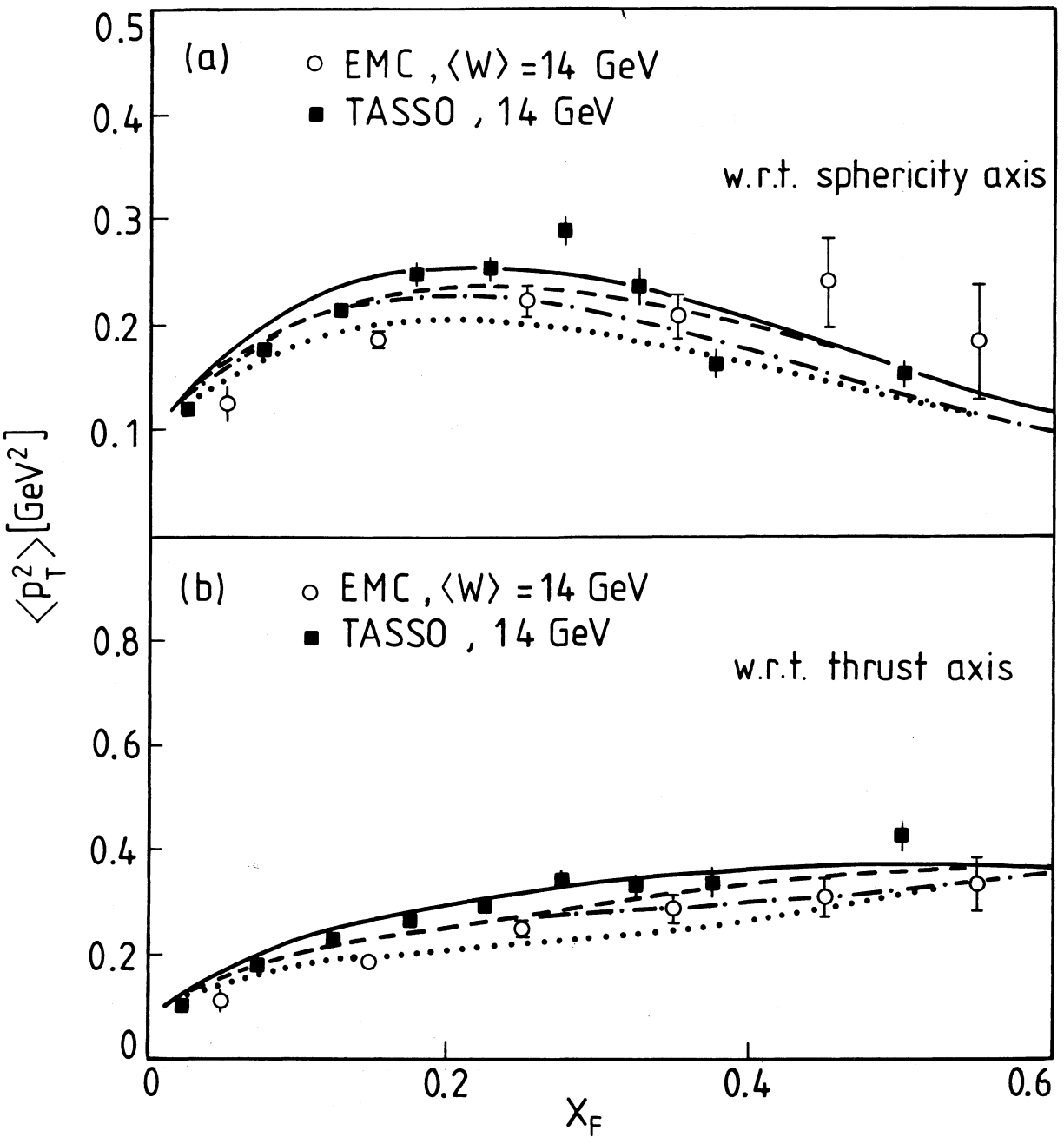
(a)
○ EMC , ⟨W⟩ =14 GeV
■ TASSO , 14 GeV
w.r.t. sphericity axis
(b)
○ EMC , ⟨W⟩ =14 GeV
■ TASSO , 14 GeV
w.r.t. thrust axis
⟨p_T^2⟩ [GeV^2]
X_F
0.5
0.4
0.3
0.2
0.1
0.8
0.6
0.4
0.2
0
0.2
0.4
0.6

FIG. 10.

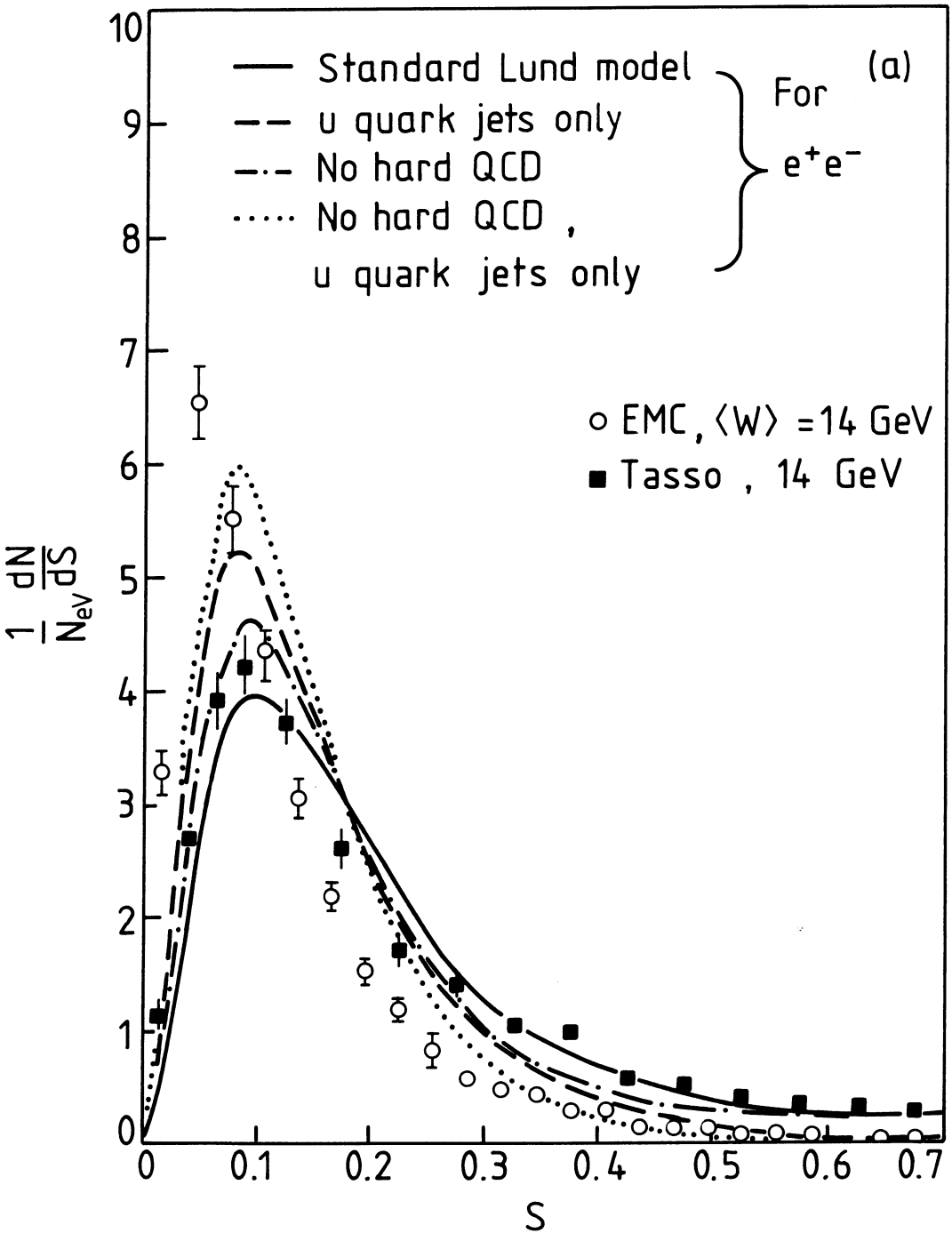
Standard Lund model
u quark jets only
No hard QCD
No hard QCD ,
u quark jets only
For
e+e−
(a)
EMC, ⟨W⟩ =14 GeV
Tasso , 14 GeV
1/N_ev dN/dS
S
0
0.1
0.2
0.3
0.4
0.5
0.6
0.7
1
2
3
4
5
6
7
8
9
10

FIG. 11 a.

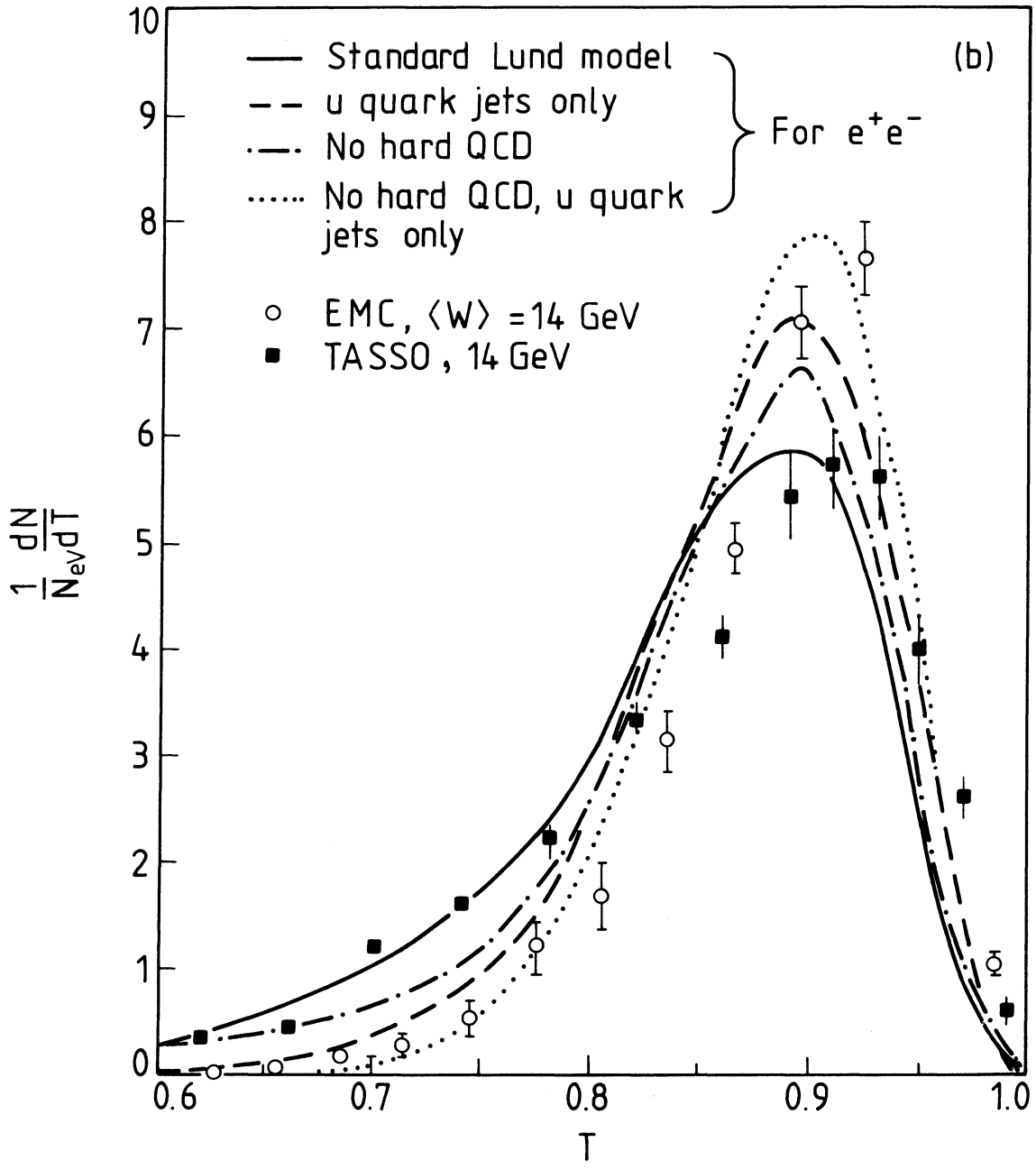
Standard Lund model
u quark jets only
No hard QCD
No hard QCD, u quark jets only
For e+e−
(b)
EMC, ⟨W⟩ =14 GeV
TASSO, 14 GeV
1/N_ev dN/dT
T
0
1
2
3
4
5
6
7
8
9
10
0.6
0.7
0.8
0.9
1.0

FIG. 11 b.

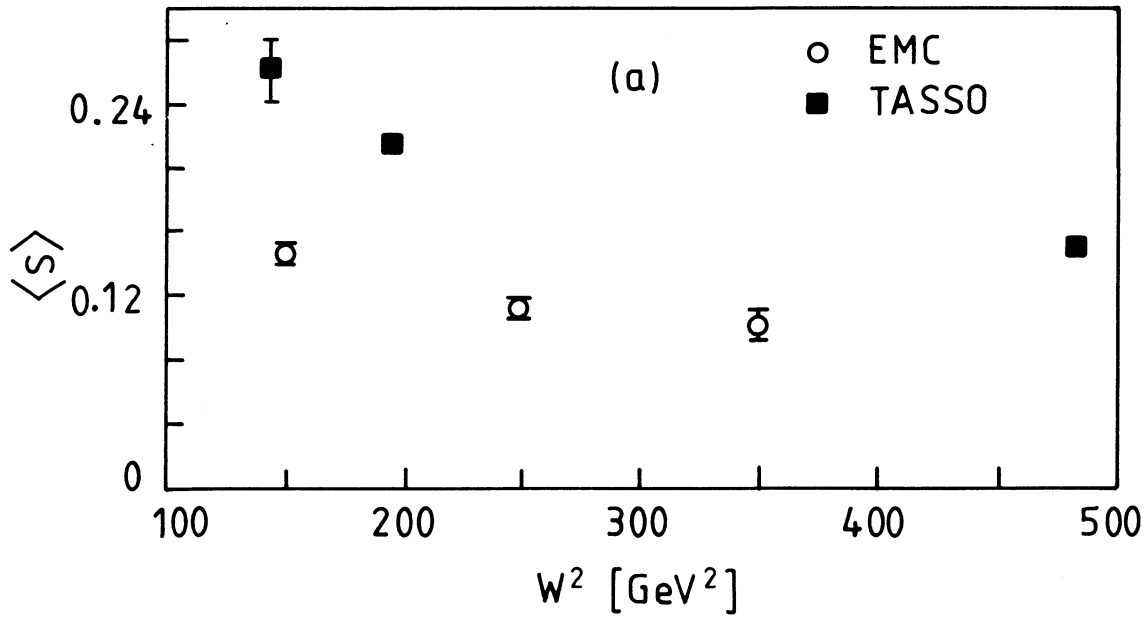
(a)
EMC
TASSO
0.24
0.12
0
⟨S⟩
100
200
300
400
500
W² [GeV²]

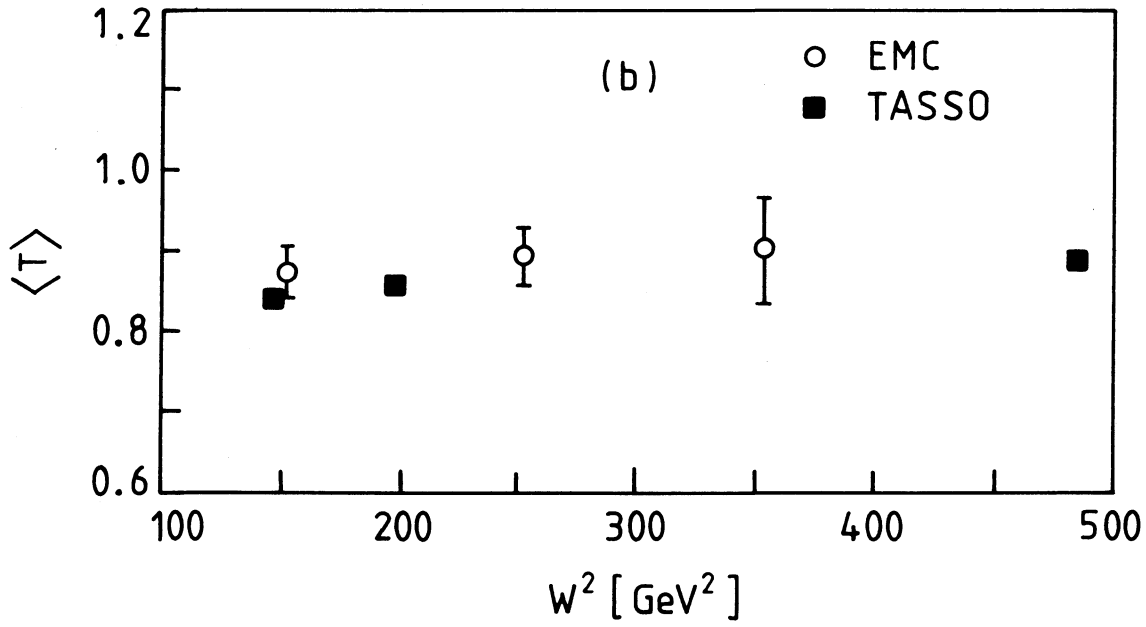
(b)
EMC
TASSO
1.2
1.0
0.8
0.6
⟨T⟩
100
200
300
400
500
W² [GeV²]

FIG. 12.

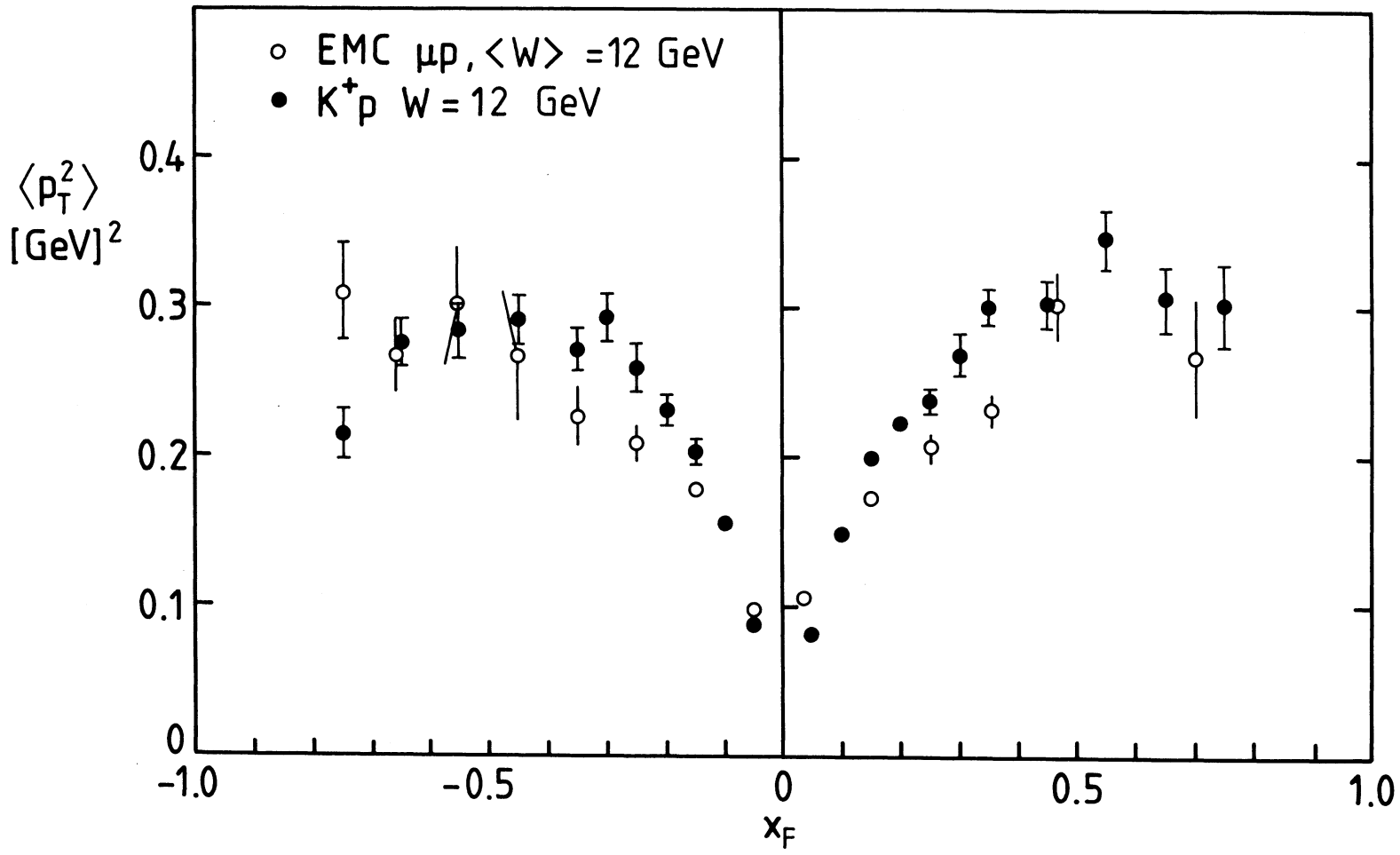


FIG. 13.